https://doi.org/10.5194/egusphere-2023-720
Preprint. Discussion started: 8 May 2023

Above- and Belowground Plant Mercury Dynamics in a Salt Marsh Estuary in Massachusetts, USA

Ting Wang[1], Buyun Du[1], Inke Forbrich[2], Jun Zhou[1], Joshua Polen[1], Elsie M. Sunderland[3], Prentiss H. Balcom[3], Celia Chen[4], Daniel Obrist[1,5*]

[1]Department of Environmental, Earth, and Atmospheric Sciences, University of Massachusetts Lowell, Lowell, MA 01854, USA

[2]Marine Biological Laboratory, Woods Hole, MA 02543, USA

[3]Harvard John A. Paulson School of Engineering and Applied Sciences, Harvard University, Cambridge, MA 02138, USA

[4]Department of Biological Sciences, Dartmouth College, Hanover, NH 03755, USA

[5]Division of Agriculture and Natural Resources, University of California, Davis, CA 95618, USA

Correspondence to: Daniel Obrist (daniel_obrist@uml.edu)

Abstract. Estuaries are dominant conduits of mercury (Hg) to the coastal ocean and the salt marshes within play an important role in coastal Hg cycling. While Hg cycling in upland terrestrial systems has been well studied, processes in salt marsh ecosystems are poorly characterized. We investigated Hg dynamics in vegetation and soils in the Plum Island Sound estuary in Massachusetts, USA and specifically assessed the role of marsh vegetation for Hg deposition and turnover. Monthly quantitative harvesting of aboveground biomass showed strong linear seasonal increases in plant Hg, with a four-fold increase in Hg concentration and an eight-fold increase in standing Hg mass between June (3.9±0.2 μg kg^{-1} and 0.7±0.4 μg m^{-2}, respectively) and November (16.2±2.0 μg kg^{-1} and 5.7±2.1 μg m^{-2}, respectively). Hg ceased to increase in aboveground biomass after plant senescence, indicating physiological controls of vegetation Hg uptake in salt marsh plants. Hg concentrations in live roots and live rhizomes were 11 times and two times higher than concentrations in aboveground live biomass, respectively. Furthermore, live belowground biomass Hg pools (roots and rhizomes, 108.1±83.4 μg m^{-2}) is more than ten times larger than peak standing aboveground Hg pools (9.0±3.3 μg m^{-2}).

A ternary mixing model suggests Hg sources in marsh aboveground tissues originates from a mix of root uptake (~35%), precipitation uptake (~33%), and atmospheric gaseous elemental mercury (GEM) uptake (~32%). The results suggest a more important role of Hg transport from belowground (i.e., roots) to aboveground tissues in salt marsh vegetation compared to upland vegetation, where GEM uptake is generally the dominant Hg source. GEM deposition via uptake and subsequent senescence (5.9 μg m^{-2} yr^{-1}) and throughfall (1.0 μg m^{-2} yr^{-1}) hence is lower in this salt marsh ecosystem compared to upland vegetation and is similar to open field wet and dry deposition (6.2 μg m^{-2} yr^{-1}). Hg contained in salt marsh aboveground tissues leads to direct Hg export to tidal water and oceans via wrack (tidal flushing of vegetation), which accounts for ~1.6 μg m^{-2} yr^{-1}. Hg consumption by herbivory ranges between 0.5 and 2.4 μg Hg m^{-2} yr^{-1}. The similarity in isotopic signatures between roots and soils suggest that belowground plant tissues mostly take up Hg directly from soils. Annual root turnover results in large internal Hg recycling between soils and plants accounting for 58.6 μg m^{-2} yr^{-1}. An initial mass balance of Hg in this whole estuarine salt marsh ecosystem considering atmospheric inputs (atmospheric GEM and precipitation Hg(II), throughfall, including plants) and losses (wrack export and lateral exchange of dissolved and particulate Hg) shows that the salt marsh presently serves as a small net Hg sink for environmental Hg of 5.2 μg m^{-2} yr^{-1}.

https://doi.org/10.5194/egusphere-2023-720
Preprint. Discussion started: 8 May 2023

1. Introduction

Coastal salt marshes are ecosystems located at the interface between terrestrial and marine ecosystems and experiencing twice daily saltwater inundation by tidal water. They provide important ecological services, have high socioeconomic benefits, and serve as sinks and sources of carbon, nutrients, and contaminants (Hopkinson et al., 2018; Morris et al., 2013). Riverine export is the largest source of mercury (Hg) to coastal oceans globally (Amos et al., 2014; Liu et al., 2021). The location of salt marshes at this interface merits an understanding of their respective Hg sinks and sources and role in coastal Hg cycling. The Plum Island Sound salt marsh in Massachusetts, USA is the largest macrotidal marsh estuary in New England and is considered a biological mercury (Hg) hotspot, with 62% of saltmarsh sparrows reportedly exceeding a blood Hg threshold that may reduce nesting success (Evers et al., 2007; Jackson et al., 2011; Lane et al., 2020; Lane et al., 2011). While there is no direct evidence of particular Hg point sources within this watershed (Wang and Obrist, 2022), possible sources in the salt marsh estuary include atmospheric deposition directly to the marsh and its watershed (Evers et al., 2007; Lane et al., 2011). A recent investigation of the salt marsh indicated high Hg concentrations in this marsh soils and showed evidence that this salt marsh ecosystem currently serves as a net source of Hg via lateral tidal Hg export to tidal water and the ocean (Wang and Obrist, 2022).

A potentially important Hg source in marshes also includes Hg uptake by plants. In terrestrial environments, plants assimilate substantial amounts of atmospheric Hg, which is subsequently transferred to soils via tissue senescence (e.g., litterfall) and wash-off (i.e., throughfall deposition; review by Zhou et al., 2021). Plant Hg uptake is generally dominated by assimilation of atmospheric gaseous elemental Hg (GEM), and global vegetation acts as a large atmospheric GEM pump to soils (Jiskra et al., 2018; Obrist et al., 2018; Zhou et al., 2021; Zhou and Obrist, 2021). In terrestrial ecosystems, Hg inputs derived from plants are the dominant Hg sources accounting for 60% to 90% of total Hg inputs (Zhou and Obrist, 2021). Salt marshes are characterized by high plant net primary productivity (NPP) driven by vascular macrophytes, with plant NPP as high and even exceeding that of terrestrial ecosystems (Marques et al., 2011;Tobias and Neubauer, 2009; Visser et al., 2018). For example, salt marsh biomass production across Atlantic and Gulf sites in the U.S. ranges from 228 to 1,335 g C m^{-2} yr^{-1} with a median value of 537 g C m^{-2} yr^{-1} (Tobias and Neubauer, 2009). By comparison, NPP across 18 productive U.S. forests ranging between 400 to 1,000 g C m^{-2} y^{-1} (He et al., 2012). As a result, salt marshes are considered strong sinks of atmospheric carbon driven by plant CO_2 assimilation (Forbrich et al., 2018).

We hypothesized that salt marsh plants in the Plum Island estuary salt marsh act as substantial sinks of atmospheric Hg via vegetative assimilation of GEM, and aimed to quantify Hg sources in salt marsh vegetation, accumulation rates, and turnover rates of Hg in salt marsh plants. The specific objectives of this study were to quantify: (i) Hg fluxes and pools associated with plant dynamics in the salt marsh and Hg associated with annual growth of aboveground tissues; (ii) transfer of Hg associate with aboveground tissues to soils during senescence; (iii) Hg turnover in belowground biomass, a potentially important flux given that belowground biomass production in salt marshes is equal to or greater than aboveground production (Blum, 1993; Morris, 2007); (iv) specific sources of Hg in salt marsh biomass tissues using stable Hg isotope signatures to evaluate the implications of biomass dynamics for salt marsh Hg cycling and atmospheric Hg deposition; and (v) an initial ecosystem Hg mass balance in this salt marsh based on our observations together with other available data sources.

2. Method

2.1. Site Description

Sampling sites WERE located in the Plum Island Sound on the northeastern coast of Massachusetts, USA (42°45'10", 70°56'46") between the Gulf of Maine and the city of Boston. The estuary is the largest marsh-dominated estuary in New England with a total

https://doi.org/10.5194/egusphere-2023-720
Preprint. Discussion started: 8 May 2023

marsh area of 60 km^2 and salt marsh area of 40 km^2 (Hopkinson et al., 2018; Millette et al., 2010). Tides are semidiurnal with an amplitude averaging 2.7 m (NOAA Tide Predictions, 2020). We focused our study on high marsh platforms, with an approximate elevation of 1.4 m above the North American Vertical Datum 88, which dominate tidal marshes in New England and account for 75% of the vegetated area in the Plum Island Sound estuary (Millette et al., 2010; Wilson et al., 2014). The high marsh exhibits poor water drainage (Wilson et al., 2014) and is generally inundated biweekly during spring tides and during major storms (Millette et al., 2010). The two dominant species on the high marsh are C4 species including *Spartina patens (*common name: marsh hay) and *S. alterniflora* (common name: smooth cordgrass), with the latter mainly distributed along tidal channels and also dominant in low marsh platforms (Anjum et al., 2012; Cheng et al., 2006; Curtis et al., 1990; Maricle et al., 2009; Sun et al., 2020). Another C4 species, *Distichlis spicata* (coastal saltgrass), is often collocated within *S. patens*-dominated sites on high marsh platforms (Arp et al., 1993), whereas *Juncus gerardii* (saltmarsh rush) usually dominates the terrestrial boundary of the high marsh (Bertness, 1991).

2.2. Vegetation and Soil Sampling and Processing

Aboveground biomass of the dominant species, *S. alterniflora* and *S. patens*, were collected every four to five weeks between June and November in 2021, corresponding to the active growing season. Additional senesced biomass was sampled in the following year in April 2022, and two additional salt marsh species, *D. spicata* and *J. gerardii*, were sampled in September 2018. For each sampling date, eight 1-m^2 square plots were selected in the footprint area of a micrometeorological flux tower (Forbrich et al., 2018), of which four squares were dominated by *S. alterniflora* and four adjacent squares were dominated by *S. patens*. During vegetation sampling, all aboveground vegetation within the 1-m^2 squares was clipped close to the ground and stored in plastic Ziploc bags in coolers over ice and subsequently in refrigerators until processing. In the laboratory, wet and dry vegetation mass was determined, vegetation was carefully separated into live and senesced tissues and prepared for analysis of Hg in both bulk samples and in individual species.

In four of the eight sampling sites, quantitative belowground sampling was performed in July 2021, with two plots dominated by *S. alterniflora* and the other two plots dominated by *S. patens*. Soil cores with diameter of 10 cm to a depth of 40 cm were taken and separated into depth increments of 0-20 cm and 20-40 cm. Belowground components were separated into the following components by washing onto a fine mesh with pore size of 0.25 mm: live roots and rhizomes identified by turgidity and color (e.g., hard and white tissues versus soft and grey/discolored); senesced roots, rhizomes, and soil detritus (not recognizable organic matter); and sediments and fine organic matter that passed through the fine mesh (only analyzed in two subsamples). All plant tissues were rinsed with tap water until the water was clean, then thoroughly rinsed three times with Milli-Q water, while a selected number of live aboveground tissues were analyzed both washed and unwashed for estimation of washable Hg (see section of throughfall estimation). All samples were dried at 65 °C for at least 76 hours until constant weight, and ground using stainless steel coffee grinders prior to analyses.

2.3. Hg concentration and stable isotope analysis of vegetation and soils samples

Total Hg concentrations in all components were measured using a tri-cell Milestone DMA-80 Direct Mercury Analyzer (Milestone Inc., Monroe, Connecticut, USA) through thermal decomposition, catalytic reduction, amalgamation, desorption, and atomic absorption spectroscopy following EPA method 7473 (U.S. EPA., 1998). The system was re-calibrated based on daily performance checks using five-point calibration curves. Standard reference materials, including NIST 1515 Apple leaves (43.2 μg kg^{-1}) and Canadian National Research Council certified reference material MESS-4 (marine sediment, 91 μg kg^{-1}), were used as continuous calibration verifications after every ten-samples. Percent recoveries of total Hg for certified reference materials averaged of 99.9

https://doi.org/10.5194/egusphere-2023-720
Preprint. Discussion started: 8 May 2023

± 5.5% (range of 89.6% to 111.4%) and all blanks were below detection limits (0.001 ng). All samples were analyzed in triplicate and results were accepted when coefficients of variation were less than 10%.

Hg stable isotopes were measured on select samples including aboveground biomass, live root, live rhizomes, and surface (0-22.5 cm) and deeper soils (97.5 cm). Samples were pre-concentrated with a Nippon direct Hg analyzer (Nippon Instruments) as described in Enrico et al. (2021). A HGX-200 cold vapor generator (Teledyne Cetac Technologies) was used to introduce sample Hg to a Thermo Neptune plus MC-ICP-MS at Harvard University. An Apex-Q nebulizer (Elemental Scientific) was used to nebulize a Thallium (Tl) solution and inject TI aerosols in the HGX-200. NIST3133 (primary standard) and RM8610 (previously UM- Almaden, secondary standard) were used as Hg isotopic standard solutions, and NIST997 (thallium isotopic standard solution) was used as the reference material to correct instrument mass bias. NIST 1515 Apple leaves and Canadian National Research Council certified reference material MESS-4 were used to verify isotope analysis, and standard recoveries were in the acceptable range (from 82% to 93%). Small delta (δ) annotation is used for mass-dependent fractionation (MDF), which is reported as per mil (‰) values relative to NIST-3133 based on equation (1),

$$\delta^{xxx}Hg = \left(\frac{(^{xxx}Hg/^{198}Hg)_{sample}}{(^{xxx}Hg/^{198}Hg)_{NIST3133}} - 1\right) \times 1000 \quad (1)$$

where ^{xxx}Hg is the mass of each Hg isotope between 199 and 204. Capital delta (Δ) annotation is used for mass-independent fractionation (MIF), describing fractionation away from the expected MDF based on equation (2),

$$\Delta^{xxx}Hg = \delta^{xxx}Hg - \beta_{xxx} \times \delta^{202}Hg \quad (2)$$

where ^{xxx}Hg denotes mass of each Hg isotope 199, 200, 201, and 204, and β_{xxx} is the constant mass-dependent correction factor (0.252, 0.502, 0.752, and 1.492, respectively; Blum and Bergquist, 2007). To determine Hg sources, a ternary isotope mixing model was used to estimate fractions of Hg in above-ground biomass. End-member Hg sources used included signatures of salt marsh plants roots, atmospheric GEM, and precipitation (see SI for details).

2.4 Data Analysis

Data were checked for normality (Shapiro–Wilk test) and homogeneity of variance assumptions of statistical tests. The non-normalized data were subjected to a natural logarithmic transformation to ensure a normal distribution. Unpaired Student t-tests were used to assess significant differences between groups (e.g., species), and statistical differences between non-washed and washed aboveground vegetation samples were performed using paired Student t-tests. Linear regression analyses were performed to determine the rate of aboveground biomass Hg uptake over time. Hg mass and turnover rates were calculated by multiplication of Hg concentrations by corresponding biomass or biomass growth and other mass components at the level of sampling plots. All statistical tests were performed with STATA (Version 16.0, Statacorps, College Station, Texas), and all regressions and statistical tests presented in text, tables, and figures were based on statistical differences with p-values < 0.05. Variability presented in the text and figures are standard deviations of means.

3. Results

3.1 Hg concentrations in aboveground and belowground biomass

Hg concentrations in aboveground tissues showed substantial seasonal variations and species-specific differences, with lowest concentrations in live tissues of *S. alterniflora* and *D. spicata*, followed by *S. patens*, and highest concentrations in *J. gerardii* (Fig 1a). Despite species differences in Hg concentrations, concentrations in bulk vegetation of communities dominated by *S.*

https://doi.org/10.5194/egusphere-2023-720
Preprint. Discussion started: 8 May 2023

alterniflora versus *S. patens* (Fig 1b) were not statistically different. This likely occurred because these communities are composed of multiple species. For example, *S. alterniflora* communities also have a presence of *S. patens* plants, and *S. patens* communities include large numbers of *D. spicata* plants. Similarly, Hg concentrations of senesced *S. patens* and *S. alterniflora* bulk samples were not statistically significantly different from each other (Fig S1).

Hg concentrations in aboveground live biomass strongly increased throughout the growing season between June and November across all species. Figure 2 shows a linear increase of Hg concentrations in live aboveground tissues in plots dominated by *S. alterniflora* and *S. patens* over time ($r^2 = 0.84$; $p < 0.01$; $n = 50$), with no significant difference in regressions between the two communities. Based on these linear regression slopes, we calculated daily uptake rates of Hg during the growing season of 0.08±0.01 μg kg^{-1} day^{-1} for both *Spartina* communities. After senescence, Hg concentrations in senesced aboveground biomass measured in spring of the following year (April 2022) were not further enhanced compared to live biomass samples collected in fall (November 2021; $p = 0.19$), (Figs 2 and 4a) so that no statistically significant Hg uptake (or loss) occurred in biomass after senescence.

We washed and separated belowground samples into the following categories: live roots, live rhizomes, combined dead roots, rhizomes, and detritus (unrecognizable biomass components), and combined fine soil mineral and humus fraction. This process was based on visual separation of tissues (Elsey-Quirk et al., 2011; Valiela et al., 1976). We observed live roots and rhizomes only in the top 20 cm of the soils with no recognizable live roots and rhizomes at 20-40 cm depth. Although aboveground Hg concentrations between the two communities were similar, Hg concentrations in live roots and rhizomes (upper 20 cm)s were two to three times higher in *S. patens* plots (258.9±70.3 μg kg^{-1} and 46.6±14.2 μg kg^{-1} respectively) compared to *S. alterniflora* plots (84.5±47.0 μg kg^{-1} and 27.9±1.1 μg kg^{-1} respectively) (Fig 3, Table S1). Compared to live tissues, we observed higher Hg concentrations in senesced roots, rhizomes, and detritus (318.0±30.1 μg kg^{-1} in *S. alterniflora*, 323.3±135.4 μg kg^{-1} in *S. patens*), which also was higher than Hg concentrations in soil mineral and humus fractions of 272.3±11.6 μg kg^{-1} (although only measured in one *S. patens* sample) (Fig 3, Table S1). Hg concentrations in senesced belowground biomass (roots, rhizomes, and detritus) were higher than that in mineral and humus samples at 20-40 cm soil depths, although with larger variation (Table S1). Bulk soil Hg concentrations (i.e., composed of all fractions listed above) averaged 194.6±28.3 μg kg^{-1} of *S. alterniflora* community and 171.2±72.1 μg kg^{-1} of *S. patens* community in the top 20 cm with no significant difference ($p>0.05$). Bulk soil Hg concentrations of the 20-40 cm soil in *S. alterniflora* (279.1±203.8 μg kg^{-1}) were almost twice that of *S. patens* (159.1±122.7 μg kg^{-1}). Overall, Hg concentrations of live roots (171.7±111.9 μg kg^{-1}) were 11 times higher and live rhizome (37.3±13.6 μg kg^{-1}) were double the concentrations of aboveground live biomass (16.2±2.0 μg kg^{-1}, Table S2).

3.2 Hg pools sizes associated with aboveground and belowground biomass

Aboveground standing live biomass strongly increased from June through August, when it plateaued at a peak biomass in August (507±208 g m^{-2}) and September (498±118 g m^{-2}, a trend that was consistent among species) (Fig 4b). Hg mass contained in live aboveground biomass peaked later (in November) than standing biomass and showed an eight-fold and near-linear increase between June (0.7±0.4 μg m^{-2}) and November (5.7±2.1 μg m^{-2}) (Fig 4c). Peak Hg pools contained in aboveground biomass were 5.7±2.1 μg m^{-2} for live tissue and 3.3±1.7 μg m^{-2} for senesced tissue, for a total combined standing aboveground biomass Hg pools of 9.0 ±3.3 μg m^{-2} in November (Figs 4c and 5). This also represents our best estimate of total annual Hg assimilation by aboveground vegetation, assuming that little standing senesced biomass in November was attributable to NPP of the previous year growing season. Standing aboveground biomass in the spring of the following year (April 2022, 357±148 g m^{-2}) was 39% lower than aboveground biomass in November of 2021 (583±208 g m^{-2}) (Fig 4b), and standing Hg pools were 32% lower in the

https://doi.org/10.5194/egusphere-2023-720
Preprint. Discussion started: 8 May 2023

subsequent spring (6.1 ±1.9 μg m^{-2}) compared to peak fall levels (9.0 ±3.3 μg m^{-2}) (Fig 4c), showing losses of standing aboveground biomass and associated Hg pools over winter.

Live root biomass in surface soils (top 20 cm) averaged 361±114 g m^{-2} and live rhizome biomass were approximately twice as large (792±231 g m^{-2}), for a combined live belowground biomass of 1,153±321 g m^{-2} (Table S2). Belowground Hg pools associated with these live tissues averaged 70.0±63.7 μg m^{-2} for roots, 38.1±22.4 μg m^{-2} for rhizomes, and 108.1±83.4 μg m^{-2} for the combined live belowground tissue, accounting for less than 0.5% of the total bulk soil Hg pool (Fig 5a, b, Table S2). We observed a much larger Hg pool associated with senesced biomass (roots, rhizomes, and detritus) averaging 4,116±1,141 μg m^{-2}, accounting for 16.1% of the total bulk soil Hg pool. We estimated a total soil Hg pool in the top 40 cm using measured bulk densities (range of 0.22 and 0.37 g cm^{-3}) exceeding 25,000 μg m^{-2}, with most of this Hg associated with fine soil mineral and humus fraction (83.5%), rather than contained in live and senesced plant tissues.

3.3 Hg stable isotope signatures to determine Hg sources

Aboveground biomass showed negative mass-dependent fractionation (MDF) values for δ^{202}Hg between -1.61‰ and -1.07‰, and mass-independent (MIF) values were consistently positive with Δ^{199}Hg between 0.20‰ and 0.43‰ and Δ^{200}Hg values between 0.04‰ and 0.11‰ (Fig 6, Tables S3 and S4). These aboveground isotopic Hg signatures of salt marsh vegetation fell outside of the range commonly reported in foliar samples of terrestrial vegetation, both regarding mass-dependent and mass-independent signatures. Specifically, terrestrial vegetation Hg signatures are substantially more negative in δ^{202}Hg values (ranging from -3.06‰ to -2.37‰ [inter-quartile range, IQR, n = 120)] and both Δ^{199}Hg and Δ^{200}Hg values in terrestrial vegetation generally show negative values (Δ^{199}Hg: -0.42‰ to -0.27‰ IQR, Δ^{200}Hg: -0.05‰ to 0.01‰, IQR) (Fig 6, Table S4) (review by Zhou et al., 2021).

Stable Hg isotope signatures of salt marsh plant roots were different from aboveground biomass, with less negative values for δ^{202}Hg (-0.75‰ and -0.66‰), less positive values for Δ^{199}Hg (0.11‰ and 0.22‰), and close to zero values (instead of positive values) for Δ^{200}Hg (-0.01‰ and 0.04‰) (Fig 6, Tables S3 and S4). The Hg isotope signatures of roots closely overlapped with signatures in surface marsh soils and deeper marsh soils (δ^{202}Hg: -0.92‰ to -0.29‰, Δ^{199}Hg: -0.09‰ to 0.20‰, and Δ^{200}Hg: -0.02‰ to 0.05‰, Tables S3 and S4). Similar to aboveground tissues, salt marsh soil isotopic Hg signatures were largely outside the ranges reported for upland soils, particularly for δ^{202}Hg values that are much more negative in upland soils (δ^{202}Hg generally between -0.5‰ and -2.9‰; review by Zhou et al., 2021). Hg isotope signatures of salt marsh rhizomes were quite variable and in-between values observed in foliage and soils. Specifically, rhizomes showed δ^{202}Hg values between -1.41‰ to -0.70‰, Δ^{199}Hg values between 0.13‰ to 0.22‰, and Δ^{200}Hg values between -0.05‰ to 0.04‰ (Fig 6, Tables S3 and S4). Finally, Δ^{201}Hg and Δ^{199}Hg across all marsh samples showed statistically significant correlations with a slope close to 1 (0.98, $p < 0.01$, Fig S2).

4. Discussion

4.1 Salt marsh vegetation and soil Hg concentrations

Strong seasonal Hg concentration increases in salt marsh aboveground tissues were consistent with patterns also observed in upland ecosystems, such as in forest foliage (Wohlgemuth et al., 2022). In upland systems, foliar Hg increases are attributed in large part to atmospheric GEM uptake, which is taken up during the growing season by stomatal and non-stomatal (i.e., cuticular) leaf uptake (review by Zhou et al., 2021). Hg uptake is controlled by leaf physiological processes and related to photosynthetic capacity, leaf nitrogen concentrations, leaf mass area, and stomatal densities and conductance (Wohlgemuth et al., 2022). In support of a similar active role of plant physiology in controlling Hg uptake in salt marsh plants, we observed that Hg concentrations in senesced biomass in April of 2022 were not significantly enhanced compared to live biomass of the previous November (2021) (Fig 2),

https://doi.org/10.5194/egusphere-2023-720
Preprint. Discussion started: 8 May 2023

indicating that no significant Hg assimilation occurred during wintertime in senesced biomass. However, increases in Hg concentrations occurred through November even after peak biomass was reached in August and September. We attribute this to continued active plant physiology through late season similar to carbon assimilation and active plant photosynthesis which continues at least through October at this site (Forbrich et al., 2018; no data is available for November). In contrast to upland plant leaves, however, stable Hg isotope signatures of marsh aboveground biomass show different Hg sources and indicate Hg uptake was not dominated by atmospheric GEM uptake (see below).

Calculated daily Hg accumulation rates in *Spartina*-dominated aboveground biomass (0.08 μg kg^{-1} day^{-1}, Fig 2) was at the lower range of foliar accumulation rates reported in forest foliage (conifer needle: median of 0.07 μg kg^{-1} day^{-1}, deciduous leaf: median of 0.23 μg kg^{-1} day^{-1}; Wohlgemuth et al., 2022). This is consistent with the notion that low-statured grassland plants generally exhibit lower Hg concentrations (5 μg kg^{-1} [1-31 μg kg^{-1}]) than trees (e.g., forest foliage (20 μg kg^{-1} [2-62 μg kg^{-1}]) (review by Zhou et al., 2021), although it may also be due to different origins of Hg (section 4.2.1 below). Both dominant marsh species in our study are C4 plants, which previous work shows have lower Hg concentrations compared to C3 species (e.g., 23±9 μg kg^{-1} versus 53±12 μg kg^{-1}, Canário et al., 2017). In laboratory studies with upland plants, leaf uptake of Hg vapor has been linked to catalase activity which is known to be lower in C4 plants (Du and Fang, 1983).

Highest Hg concentrations in *S. alterniflora* and *S. patens* were observed in fall (11.7 μg kg^{-1} and 24.0 μg kg^{-1}, respectively). Hg concentrations fell within concentration ranges reported from other uncontaminated marsh halophytes (Table S6), such as 5 to 33 μg kg^{-1} in the Great Bay estuary in New Hampshire, USA (Heller and Weber, 1998), an average of 20 μg kg^{-1} in Big Sheepshead Creek estuary in New Jersey USA (Kraus et al., 1986), and 3 to 79 μg kg^{-1} in the Ria de Aveiro Coastal Lagoon, Portugal (Anjum et al., 2011). Hg concentrations in aboveground tissues in our study, however, were much lower than those from contaminated marshes where concentrations up to 90 μg kg^{-1} were observed in the Hackensack Meadowlands in New Jersey (Windham et al., 2001) and up to 160±70 μg kg^{-1} in Piles Creek in New Jersey (Kraus et al., 1986) and even up to 1124 ± 21 μg kg^{-1} in Tagus estuary, Portugal (Canário et al., 2017). Lower Hg concentrations (10.2 ± 0.9 μg kg^{-1}) were reported from the polluted Yangtze River estuary (Wang et al., 2021).

In contrast to upland plants, salt marsh plants (including both *Spartina* species) have salt glands which are used for selective and active excretion of sea salt (Kirschner and Zinnert, 2020; Maricle et al., 2009). Salt glands also have been linked to excretion of metals (Weis and Weis, 2004), and previous studies reported correlations between leaf surface Hg and sodium (Na) release in *S. alterniflora* suggesting active Hg excretion by salt glands (Weis and Weis, 2004; Windham et al., 2001). Windham et al. (2001) proposed that in the Hackensack Meadowlands, a polluted salt marsh ecosystem, seasonal declines in Hg concentrations in *S. alternifla* leaves between May (90 μg kg^{-1}) to July (30 μg kg^{-1}) were driven by strong leaf excretion of Hg. By washing leaves of a select number of samples, we found that washing removed about 6% of total leaf Hg in *S. alterniflora* and 16% in *S. patens*, respectively (Table S5, note that we use the wash-off fraction as an estimate of throughfall deposition in the mass balance estimation below). The relatively minor loss of Hg associated with washing showed that most leaf Hg was structural and likely internal Hg, which along with observed seasonal Hg concentration increases does not support substantial seasonal Hg losses nor seasonal concentration declines which would be attributable to salt excretion at this site.

Hg concentrations in live roots and rhizomes at our sites were much higher (11 and two times, respectively) than aboveground live biomass concentrations. This is consistent with previously reported data that also reported higher root Hg concentrations in salt marshes (Anjum et al., 2012; Cabrita et al., 2019; Canário et al., 2017; Garcia-Ordiales et al., 2020; Weis and Weis, 2004; Windham et al., 2003). Hg concentrations were higher in live roots of *S. patens* (258.9±70.3 μg kg^{-1}) compared to *S. alterniflora* (84.5±47.0 μg kg^{-1}) (Fig 3, Table S1). A possible reason for this is finer roots in *S. patens* (personal observation), and hence higher surface to volume ratios, which may facilitate soil Hg uptake. In upland ecosystems, fine root Hg concentrations were reported to be higher

https://doi.org/10.5194/egusphere-2023-720
Preprint. Discussion started: 8 May 2023

than in coarse roots as well (Wang et al., 2012; Wang et al., 2020). Elevated root and rhizome Hg concentrations compared to aboveground tissues in marsh plants contrast with upland studies that generally report higher concentrations in foliage (20 μg kg kg^{-1} [2–62 μg kg^{-1}]) and much lower concentrations in roots (7 μg kg^{-1} [2–70 μg kg^{-1}]) (Zhou et al., 2021). An exception to this are grassland systems where root Hg concentrations also have been reported higher than foliage, although the difference was much smaller (e.g., roots: 41±31 μg kg^{-1}; leaves: 20±10 μg kg^{-1}; (Zhou and Obrist, 2021)). Our data also showed much lower root Hg concentrations in this marsh compared to a moderately contaminated estuary in Portugal (Anjum et al., 2012; Canário et al., 2017; Garcia-Ordiales et al., 2020), with the exception of lower root Hg in a contaminated salt marsh roots in the Yangtze River estuary (Wang et al., 2021) (Table S6). Overall, the reported results suggest a large range of Hg concentrations in belowground salt marsh biomass, which likely is dependent on soil Hg concentrations as the dominant Hg source for root Hg (see section 4.2.1 below). Much higher concentrations of root and rhizomes in belowground tissues compared to aboveground biomass also suggests limited translocation between belowground and aboveground tissues (Cavallini et al., 1999; Clemens and Ma, 2016; Graydon et al., 2009; Wang et al., 2012) and possibly different sources between the two (as discussed below).

4.2 Stable Hg isotope signatures and possible origins of Hg in salt marsh vegetation and soil

4.2.1 Salt marsh vegetation

One of the largest MDF processes in the environmental systems is due to preferential uptake of light atmospheric GEM isotopes by vegetation foliage that leads to large negative δ^{202}Hg signatures (generally below -2‰) and mass independent signatures similar to that of atmospheric GEM (Demers et al., 2013; Enrico et al., 2016; Yu et al., 2016). In terrestrial ecosystems, studies have shown that the vegetation uptake of atmospheric GEM and subsequent litterfall, throughfall, and plant senescence serves as the primary source of Hg loading (Demers et al., 2013; Jiskra et al., 2015; Louis et al., 2001; Obrist et al., 2017; Wang et al., 2016; Zheng et al., 2016; Zhou et al., 2021). Aboveground biomass of salt marsh plants show a distinctly different signature than reported patterns from upland foliage. Specifically, MDF values were much less negative, and values of odd-MIF (Δ^{199}Hg) and even-MIF (Δ^{200}Hg) were more positive, compared to upland foliage (Fig 6, Table S4). We propose that salt marsh plant leaves have distinctly different sources than the dominant atmospheric GEM uptake proposed in upland plants. The similarities of the two MIF patterns (Δ^{199}Hg and Δ^{200}Hg) further suggest that the difference is largely due to different sources (i.e. end-member mixing) as opposed to process-based fractionation processes after uptake (review by Kwon et al., 2020).

Hg signatures of salt marsh aboveground tissue were close to signatures of salt marsh soils, yet with slightly more negative δ^{202}Hg values and more positive Δ^{199}Hg and Δ^{200}Hg values (Table S4). We used a ternary mixing model to identify Hg sources and further quantify their contributions for salt marsh plant leaves based on MDF (δ^{202}Hg) and even-MIF (Δ^{200}Hg) (Demers et al., 2013; Jiskra et al., 2021; Jiskra et al., 2017; Obrist et al., 2017). Briefly, the dominant three end-member Hg sources include: (1) direct uptake from marsh plant roots, (2) atmospheric GEM uptake through leaf stomata, and (3) precipitation Hg(II) deposition.

Our best estimate shows that the Hg source in salt marsh vegetation consists of a mixture of atmospheric GEM of 32%, root uptake of 35%, and precipitation deposition of around 33%. Most notably, the biggest difference compared to upland plants is much less negative δ^{202}Hg values. We propose that some uptake of atmospheric GEM leads to δ^{202}Hg values that are more negative than the δ^{202}Hg of plant roots and soils. Precipitation, on the other hand, which largely consists of oxidized Hg, shows a typical positive anomaly in Δ^{200}Hg linked to upper atmosphere GEM oxidation (Enrico et al., 2016; Jiskra et al., 2021; Zhou et al., 2021). We propose that precipitation contributions caused a partial Δ^{200}Hg anomaly in salt marsh aboveground biomass compared to soil sources. Our results suggest a more important role of Hg transport from belowground (i.e., roots) to aboveground tissues in salt marsh vegetation compared to upland ecosystems that report minor translocation of Hg from belowground to aboveground tissues (generally below 5% of leaf Hg originating from soils via root uptake, review by Zhou et al., 2021). Vegetation studies from salt

https://doi.org/10.5194/egusphere-2023-720
Preprint. Discussion started: 8 May 2023

marshes previously suggested inconsistent leaf Hg source patterns. For example, an Hg isotope tracer study suggested minor root-to-leaf transport with soils accounting for a small percentage of Hg in marsh plants (i.e. 2.2-2.7% from Cabrita et al. (2019)), while a study based on bioaccumulation factors suggested a wide and inconstant range of soil Hg contribution to leaves from 1.7-9.6 % to as high as 46% (Castro et al., 2009).

The mixing model results were not able to fully match the range of odd-MIF (Δ^{199}Hg) due to more positive Δ^{199}Hg signatures in salt marsh plant leaves, and it is possible that chemical and biological processes modify original salt marsh vegetation isotope signatures after uptake. For example, odd-MIF signature is impacted by photochemical reductions of aqueous inorganic Hg(II) inducing more positive values (Bergquist and Blum, 2007; Kwon et al., 2014; Meng et al., 2019; Yuan et al., 2019). Relationships between two odd-MIF, Δ^{201}Hg and Δ^{199}Hg, are used to assess photoreduction pathways (Bergquist and Blum, 2007), and we observed a positive correlation between Δ^{201}Hg and Δ^{199}Hg across salt marsh samples (slope of 0.98; Fig S2), which is in large parts driven by leaves with higher values of both Δ^{201}Hg and Δ^{199}Hg values. This slope is close to a slope reported during inorganic Hg(II) photoreduction (slope of 1.00) (Bergquist and Blum, 2007; Blum et al., 2014), so that it is possible that photochemical reduction of Hg in exposed leaves may contribute to isotopic patterns.

Roots of salt marsh plants show a Hg isotope signature that almost perfectly overlaps the signatures observed in soils, strongly suggesting a dominant soil source. In terrestrial plants, Hg assimilated in belowground biomass also is considered largely of soil origin with little internal translocations of Hg from aboveground tissues (Millhollen et al., 2006; Obrist et al., 2018; Zhou et al., 2021). This also has been proposed in aquatic plants (e.g., mangroves, sawgrass) where root Hg largely derives from surrounding soils (Huang et al., 2020; Mao et al., 2013; Yin et al., 2013). Dominant soil Hg sources in roots would also explain the differences in root Hg levels with salt marsh contamination levels as discussed above. Finally, rhizome Hg isotope signatures indicate a mix of above-ground and belowground Hg sources, although they show a large variation in isotope signatures with some samples being closer to aboveground tissue and others being closer to root signatures. This observation is consistent with the role of rhizomes as storage organs with over one year lifetime, whereby carbohydrates and nutrients are mobilized via rhizomes between above- and belowground organs based on plant allocation needs.

4.2.2 Salt marsh soil

The salt marsh soil isotope signature fell almost completely outside the range of soil Hg signatures reported from upland studies. In terrestrial environments, the strong MDF during foliar GEM uptake imprints a similar and typical terrestrial fingerprint on soil Hg, resulting in soil signatures with strong negative δ^{202}Hg and Δ^{200}Hg values similar to that of vegetation. Mixing models based on isotopic Δ^{200}Hg data suggest upland soil Hg sources are dominated by atmospheric GEM (accounting for 53% to 92% of the source), which originates from plant Hg uptake and subsequent deposition (e.g., plant senescence) of overlying vegetation (Jiskra et al., 2018; Obrist et al., 2018; Zhou et al., 2021; Zhou and Obrist, 2021). These upland soil Hg isotope signatures propagate in watershed runoff (Jiskra, et al., 2017; Woerndle et al., 2018). Soils of our salt marsh study notably lacked the strong δ^{202}Hg depletion signal of uplands soils (e.g., δ^{202}Hg of marsh soils between -0.92‰ and -0.29‰, versus -0.5‰ to -2.5‰ in other soils, review by Zhou et al., 2021) and further supports that the source of Hg in marsh vegetation, which ultimately deposits to soils, is distinctly different from that of upland ecosystems. The isotopic signature of soil samples in Figure 6a also does not support a simple two-way mixing between plant and precipitation Hg to explain salt marsh soils Hg signatures. Further terrestrial surface runoff, which generally shows typical terrestrial origin signatures (but was not measured in our study), also cannot explain marsh soil Hg isotope patterns.

Hg isotopic signatures of this marsh soils strongly overlap within both ocean signatures as well as with reported industrial and legacy contamination that are additional potential Hg sources in salt marsh soils. Mixing models, however, cannot be used to

https://doi.org/10.5194/egusphere-2023-720
Preprint. Discussion started: 8 May 2023

calculate their potential contributions due to very large variations of these end-member Hg sources that overlap with the signatures in soils. Seawater regularly floods the salt marsh during spring tides and storms and provide solids for salt marsh soils (Millette et al., 2010). Recently reported ocean water Hg isotopes show total Hg median values for Δ^{200}Hg of 0.02‰ (-0.01‰ to 0.03‰ IQR), while ocean particulate Hg showed similar (albeit more variable) patterns (Jiskra et al., 2021). Adding salt marsh vegetation Hg isotope signatures to those of ocean water reported by, we observe a strong overlap of salt marsh soil with ocean signatures, whereby both Δ^{200}Hg and δ^{202}Hg fall between the ranges reported for seawater (Fig S3, note that due to large variability, we were unable to quantify respective source fractions). The notion of ocean Hg sources would be consistent with a sediment mass balance study which showed that sediment loads were dominated by ocean sediments in the Plum Island Sound estuary salt marsh (Hopkinson et al., 2018), with relatively minor import of sediments derived from the watershed. Industrial and legacy contamination sources also may shape salt marsh soil Hg signatures. Industrial Hg isotope signatures are characterized by large ranges of negative δ^{202}Hg values and near-zero to positive Δ^{199}Hg and Δ^{200}Hg values (Fig S3, Table S4, see SI for details).

4.3 Hg mass balance and turnover fluxes associated with biomass dynamics.

4.3.1 Aboveground

Aboveground biomass turnover normally dominates atmospheric Hg deposition in terrestrial systems, For example, across 16 states in the eastern U.S., median annual aboveground litterfall Hg deposition, ultimately deriving from GEM uptake, was 11.7 μg m^{-2} yr^{-1} (range of 2.2-23.4 μg m^{-2} yr^{-1}) and exceeded annual wet Hg deposition by rain (median of 9.2 μg m^{-2} yr^{-1}; range of 4.5-19.7 μg m^{-2} yr^{-1}) (Risch et al., 2017). The implication of aboveground tissue turnover for Hg cycling in salt marshes are likely distinctly different from terrestrial systems due to different Hg sources. Estimated annual aboveground Hg assimilation by salt marsh plants is 9.0±3.3 μg m^{-2} yr^{-1}. Of this turnover, however, our stable isotope data suggest that about 65% (i.e., 5.9±2.1 μg m^{-2} yr^{-1}) constitutes an external source from atmospheric GEM uptake and from precipitation, and the rest (35%, 3.1±1.1 μg m^{-2} yr^{-1}) likely originates from soil uptake and hence represents an internal plant-soil recycling of Hg within the ecosystem.

Based on these results, we estimate here a mass balance of Hg sources and sinks associated with aboveground vegetation dynamics and turnover and compare these with previously reported fluxes such as lateral tidal exchanges, published wet and gaseous oxidized Hg, and particulate Hg deposition. Hg inputs to this salt marsh include wet Hg deposition, which based on interpolated data by the NADP program is estimated at 5.2 μg m^{-2} yr^{-1} (NADP, 2017), while a lower estimate of 2.9 μg m^{-2} yr^{-1} has been measured at a nearby coastal site on Cape Cod, Massachusetts (Engle et al., 2010). Combining these two data sets, we estimate a mid-point wet deposition of 4.1 μg m^{-2} yr^{-1}. Gaseous oxidized Hg (GOM) and particulate Hg (PHg) deposition in this area was estimated at 1.2 μg m^{-2} yr^{-1} based on measurements by Engle et al. (2010) and at 3.0 μg m^{-2} yr^{-1} at a deciduous forest (Harvard Forest) in Massachusetts (Obrist et al., 2021). Hence, a mid-point dry deposition of combined GOM and PHg is estimated at 2.1 μg m^{-2} yr^{-1} (Table 1, Fig 7). Aboveground vegetation Hg dynamics yields a total turnover of 9.0±3.3 μg m^{-2} yr^{-1} (combined live and senesced biomass at the end of the growing season), including 5.9±2.1 μg m^{-2} yr^{-1} constitutes an atmospheric GEM source and root uptake represents 3.1±1.1 μg m^{-2} yr^{-1}. Based on sample washing, an additional 11% of foliar Hg concentrations was subject to wash-off so that we constrain throughfall deposition of Hg to 1.0±0.4 μg m^{-2} yr^{-1}. Combined atmospheric Hg deposition attributable to aboveground vegetation hence yields 6.9 μg m^{-2} yr^{-1}, and is closer to the combined wet, GOM, and PHg deposition (6.2 μg m^{-2} yr^{-1}). Combined atmospheric Hg sources in this system are estimated at 13.1 μg m^{-2} yr^{-1} (Table 1; a range of 7.7 to 19.5 μg m^{-2} yr^{-1}).

Aboveground vegetation also results in lateral exchange of Hg between marsh and tidal water via wrack export, i.e., losses of plants and surface litter through tidal flushing. Although difficult to measure, wrack export in this area is composed primarily of *S. alterniflora* plants (Hartman et al., 1983) and has been estimated to constitute 16-19% (mid-point of 17.5%) of biomass that accumulates from NPP in the marsh (Duarte, 2017; Duarte and Cebrián, 1996). Hence, we estimate that of the annual Hg uptake

https://doi.org/10.5194/egusphere-2023-720
Preprint. Discussion started: 8 May 2023

by aboveground biomass (of 9.0 ±3.3 μg m^{-2} yr^{-1}) about 1.6 μg m^{-2} yr^{-1} (range of 1.4-1.7 μg Hg m^{-2} yr^{-1}) may be subject to wrack export. Scaling to the whole salt marsh area, the total wrack export from this marsh is estimated around 0.06 kg yr^{-1} (range of 0.06-0.07 kg yr^{-1}). In a previous study, we quantified Hg exports from the salt marsh system via tidal exchanges of dissolved and particulate Hg (without plants), and estimated 0.7 μg m^{-2} yr^{-1} of dissolved Hg export and 5.6 μg m^{-2} yr^{-1} of particulate Hg export from the marsh to the tidal water (Wang and Obrist, 2022). Our estimated annual Hg export by wrack is higher than lateral export of dissolved Hg, but much smaller than lateral export of particulate Hg. Considering all these inputs and outputs, we estimate a net present-day Hg mass accumulation in this salt marsh ecosystem between 0-11.5 μg m^{-2} yr^{-1} with a mid-point of 5.2 μg m^{-2} yr^{-1}, suggesting that this salt marsh currently represents a small net sink of environmental Hg.

It is noteworthy that the timing of aboveground tissue turnover in salt marshes occurred later than that of upland forests that have litterfall Hg inputs mainly in the fall. We observed relatively slow losses of senesced biomass over winter, whereby standing senesced aboveground biomass in spring of the subsequent year (April of 2022 357±148 g m^{-2}) was only 39% lower than peak aboveground biomass in November of 2021 (583±208 g m^{-2}, Fig 4b). Zawislanski et al. (2001) similarly reported that 32% to 39% of leaf mass was still attached to stems seven months after senescence in *S. alterniflora* stands in May of the subsequent year compared to the previous September. Senesced biomass finally is incorporated into soils, exported as wrack to the ocean, lost to decomposition, or subject to herbivory. Zawislanski et al. (2001) summarized studies and discussed that a large part of NPP (60% to 80%) accumulated in salt marsh soils; Duarte (2017) and Duarte and Cebrián (1996) suggested that the largest component of NPP (43%) was decomposing in the system, 14-17% of NPP was subject to long-term burial, and smaller amounts were subject to ocean export as wrack (16-19% of NPP) and consumed by herbivores (27%;). Another study estimated NPP loss due to herbivory of 5% (Mann, 1988). Based on these studies, we estimate that of the annual Hg mass assimilated in aboveground biomass, the largest fraction (57% to 80%, equivalent to 5.1-7.2 μg Hg m^{-2} yr^{-1}) remained in the system and was subject to net accumulation and decomposition, 16-19% (1.4-1.7 μg Hg m^{-2} yr^{-1}) was subject to wrack export, and 5% to 27% (0.5-2.4 μg Hg m^{-2} yr^{-1}) was subject to herbivory.

4.3.2 Belowground

Many studies show that in salt marsh ecosystems, belowground productivity generally is equal or greater than aboveground biomass production, and this particularly applies for northern marshes (Blum, 1993; Morris, 2007; Tobias and Neubauer, 2019; Windham, 2001). Roots of both dominant species can grow to length of 8 to 20 cm (Blum, 1993; Muench and Elsey-Quirk, 2019). *S. alterniflora* normally has large and thick rhizomes (normally ranging from 2-4 mm in diameter) with aerenchyma tissues to transport oxygen to submerged belowground tissue for respiration, while *S. patens* has relatively dense and fine roots with limited aerenchyma tissue which cannot support aerobic respiration when completely flooded (Muench and Elsey-Quirk, 2019). Live root biomass (upper 40 cm) of 444±87 g m^{-2} in *S. patens* and 278±61 g m^{-2} in *S. alterniflora* cores (Table S1), is consistent with reported denser root biomass in *S. patens* compared to *S. alterniflora* (Muench and Elsey-Quirk, 2019). Combined live roots and rhizome biomass averaged 1,153±321 g m^{-2}, and thereby exceeded peak standing aboveground biomass of 830±415 g m^{-2} in August 2021. Scaling up Hg pools using these belowground biomass data and measured Hg concentrations yields large belowground Hg pools. For example, the live belowground Hg pool (roots and rhizomes) is 108.1±83.4 μg m^{-2} and more than ten times larger than peak standing aboveground Hg pools (9.0±3.3 μg m^{-2}) (Fig 5a, Table S2). The Hg pool associated with senesced biomass (roots, rhizomes, and detritus) was over an order of magnitude larger (4,116±1,141 μg m^{-2}).

Turnover times of salt marsh macrophyte roots are estimated at 0.6 yr^{-1} (0.2 to 1.9 yr^{-1}) (Ouyang et al., 2017) and 0.5 yr^{-1} (Blum, 1993), although longer turnover times have been proposed for creek-side plants (2.6 yr^{-1} , Blum, 1993). Assuming a belowground biomass turnover rate of 0.6 yr^{-1} (0.2 to 2.6 yr^{-1}), estimated Hg mass turnover associated with belowground biomass (root and

https://doi.org/10.5194/egusphere-2023-720
Preprint. Discussion started: 8 May 2023

rhizome) is 58.6 µg m^{-2} yr^{-1} (19.5 to 253.8 µg m^{-2} yr^{-1}) (Table 1, Fig 7). Hence, belowground Hg turnover via plant tissues exceeds that of aboveground tissue (9.0±3.3 µg m^{-2} yr^{-1}) by a factor five, although it is largely unclear what the implications of this turnover may be. Given that we consider the source of belowground tissue Hg to be largely from soil uptake, this large Hg belowground turnover flux does not provide an external source and represents internal recycling of Hg between soils and belowground tissues. This recycling of Hg may have been various consequences, such as impacting mobility and bioavailability, phytostabilization by roots (Anjum et al., 2011), or remobilization of Hg associated with root decomposition.

5. Summary and conclusion

Measurements of Hg concentrations, fluxes, and turnover associated with vegetation in a salt marsh ecosystem with high above- and belowground NPP showed an annual Hg uptake in aboveground tissues of 9.0 ±3.3 µg m^{-2} yr^{-1}. Using a stable Hg isotope mixing model, we estimate that 35% of aboveground Hg originates from soil Hg uptake, 32% is from atmospheric GEM uptake, and 33% is from precipitation Hg(II) deposition. Estimated annual plant-derived atmospheric Hg deposition from plant senescence (i.e., litterfall) is estimated at 5.9±2.1 µg m^{-2} yr^{-1}, which is about half of that in forests where plant Hg assimilation of atmospheric GEM is the dominant Hg source. We estimate an additional atmospheric Hg deposition by throughfall of 1.0±0.4 µg m^{-2} yr^{-1}, for combined plant-derived Hg inputs of 6.9 µg m^{-2} yr^{-1}. This deposition is similar to combined wet and dry deposition of other atmospheric Hg forms. Seasonal and temporal Hg concentration and mass balance dynamics show strong seasonal increases during active growing season and a lack of concentration changes after senescence over winter, suggesting physiologically controlled uptake pathways. Hg contained in aboveground tissues lead to an annual wrack export (losses to tidal flushing) of 1.6 µg m^{-2} yr^{-1} to tidal water and ocean and herbivory of Hg in a range of 0.5 to 2.4 µg Hg m^{-2} yr^{-1}(Table 1, Fig 7). The remainder of vegetation Hg is slowly incorporated into soils over winter and during the subsequent year.

Belowground Hg pools associated with live tissues collected in July (108.1±83.4 µg m^{-2}) were over ten times larger than peak aboveground Hg pools and resulted in a substantial annual Hg turnover flux of 58.6 µg m^{-2} yr^{-1}. The source of root Hg is largely from soil uptake, while belowground rhizomes show variable sources both from aboveground and root tissues. The turnover of Hg associated with belowground tissues largely reflects internal recycling between soils and plants, with poorly understood impacts on Hg partitioning, bioavailability, and mobility. Hg associated with roots and rhizomes only accounted for about 0.4% of total belowground Hg pools, with the largest soil Hg pools associated with fine soil mineral and humus fractions (83.5%). Overall, we estimate this marsh to presently serve as a small net Hg sink for environmental Hg of 5.2 µg m^{-2} yr^{-1}.

6. Competing interests

The contact author has declared that none of the authors has any competing interests.

7. Acknowledgements

We thank Keely O'Beirne, Madison Sachs, and Silas Bollen for help with vegetation sampling and laboratory analysis of initial plant and soil mercury samples. We thank Nancy Pau and the Parker River National Wildlife Refuge for sampling permits and acces. We thank Samuel Kelsey, Anne Giblin and other researchers from the Plum Island Ecosystem Long-Term Ecological Research project for support and information about the estuary. Funding was provided by an award from the U.S. National Science Foundation Division of Environmental Biology (Award Number: 2027038).

https://doi.org/10.5194/egusphere-2023-720
Preprint. Discussion started: 8 May 2023

Reference

Amos, H. M., Jacob, D. J., Kocman, D., Horowitz, H. M., Zhang, Y., Dutkiewicz, S., … Sunderland, E. M. (2014). Global biogeochemical implications of mercury discharges from rivers and sediment burial. *Environmental Science and Technology*, *48*(16), 9514–9522. https://doi.org/10.1021/es502134t

Anjum, N. A., Ahmad, I., Válega, M., Pacheco, M., Figueira, E., Duarte, A. C., … Figueira, E. (2012). Salt marsh macrophyte Phragmites australis strategies assessment for its dominance in mercury-contaminated coastal lagoon (Ria de Aveiro, Portugal). *Environ Sci Pollut Res*, *19*, 2879–2888. https://doi.org/10.1007/s11356-012-0794-3

Anjum, N. A., Ahmad, I., Válega, M., Pacheco, M., Figueira, E., Duarte, A. C., & Pereira, E. (2011). Impact of seasonal fluctuations on the sediment-mercury, its accumulation and partitioning in Halimione portulacoides and Juncus maritimus collected from Ria de Aveiro coastal lagoon (Portugal). *Water, Air, and Soil Pollution*, *222*(1–4), 1–15. https://doi.org/10.1007/s11270-011-0799-4

Arp, W. J., Drake, B. G., Pockman, W. T., Curtis, P. S., & Whigham, D. F. (1993). Manual of the Vascular Flora of the Carolinas. *Vegetatio*, *104*(105), 133–143. https://doi.org/20029742

Bergquist, B. A., & Blum, J. D. (2007). Mass-dependent and -independent fractionation of Hg isotopes by photoreduction in aquatic systems. *Science*, *318*(5849), 417–420. https://doi.org/10.1126/science.1148050

Bertness, M. D. (1991). Zonation of Spartina patens and Spartina alterniflora in a New England salt marsh. *Ecology*, *72*(1), 138–148. https://doi.org/10.2307/1938909

Blum, J. D., & Bergquist, B. A. (2007). Reporting of variations in the natural isotopic composition of mercury. *Analytical and Bioanalytical Chemistry*, *388*(2), 353–359. https://doi.org/10.1007/s00216-007-1236-9

Blum, J. D., Sherman, L. S., & Johnson, M. W. (2014). Mercury isotopes in earth and environmental sciences. *Annual Review of Earth and Planetary Sciences*, *42*, 249–269. https://doi.org/10.1146/annurev-earth-050212-124107

Blum, L. K. (1993). Spartina alterniflora root dynamics in a Virginia marsh. *Marine Ecology Progress Series*, *102*, 169–178.

Cabrita, M. T., Duarte, B., Cesário, R., Mendes, R., Hintelmann, H., Eckey, K., … Canário, J. (2019). Mercury mobility and effects in the salt-marsh plant Halimione portulacoides: Uptake, transport, and toxicity and tolerance mechanisms. *Science of The Total Environment*, *650*, 111–120. https://doi.org/10.1016/j.scitotenv.2018.08.335

Canário, J., Poissant, L., Pilote, M., Caetano, M., Hintelmann, H., & O'Driscoll, N. J. (2017). Salt-marsh plants as potential sources of Hg0 into the atmosphere. *Atmospheric Environment*, *152*, 458–464. https://doi.org/10.1016/j.atmosenv.2017.01.011

Castro, R., Pereira, S., Lima, A., Corticeiro, S., Válega, M., Pereira, E., … Figueira, E. (2009). Accumulation, distribution and cellular partitioning of mercury in several halophytes of a contaminated salt marsh. *Chemosphere*, *76*(10), 1348–1355. https://doi.org/10.1016/j.chemosphere.2009.06.033

Cavallini, A., Natali, L., Durante, M., & Maserti, B. (1999). Mercury uptake, distribution and DNA affinity in durum wheat (Triticum durum Desf.) plants. *Science of the Total Environment*, *243–244*, 119–127. https://doi.org/10.1016/S0048-9697(99)00367-8

Cheng, X., Luo, Y., Chen, J., Lin, G., Chen, J., & Li, B. (2006). Short-term C4 plant Spartina alterniflora invasions change the soil carbon in C3 plant-dominated tidal wetlands on a growing estuarine Island. *Soil Biology and Biochemistry*, *38*(12), 3380–3386. https://doi.org/10.1016/j.soilbio.2006.05.016

Clemens, S., & Ma, J. F. (2016). Toxic Heavy Metal and Metalloid Accumulation in Crop Plants and Foods. *Annual Review of Plant Biology*, *67*, 489–512. https://doi.org/10.1146/annurev-arplant-043015-112301

Curtis, P. S., Balduman, L. M., Drake, B. G., & Whigham, D. F. (1990). Elevated Atmospheric CO2 Effects on Belowground Processes in C3 and C4 Estuarine Marsh Communities. *Source: Ecology*, *71*(5), 2001–2006.

Demers, J. D., Blum, J. D., & Zak, D. R. (2013). Mercury isotopes in a forested ecosystem: Implications for air-surface exchange

dynamics and the global mercury cycle. *Global Biogeochemical Cycles*, *27*(1), 222–238. https://doi.org/10.1002/gbc.20021

Du, S., & Fang, S. C. (1983). Catalase activity of C3 and C4 species and its relationship to mercury vapor uptake. *Environmental and Experimental Botany*, *23*(4), 347–353. https://doi.org/10.1016/0098-8472(83)90009-6

Duarte, C. M. (2017). Reviews and syntheses: Hidden forests, the role of vegetated coastal habitats in the ocean carbon budget. *Biogeosciences*, *14*(2), 301–310. https://doi.org/10.5194/bg-14-301-2017

Duarte, C. M., & Cebrián, J. (1996). The fate of marine autotrophic production. *Limnology and Oceanography*, *41*(8), 1758–1766. https://doi.org/10.4319/LO.1996.41.8.1758

Elsey-Quirk, T., Seliskar, D. M., & Gallagher, J. L. (2011). Nitrogen Pools of Macrophyte Species in a Coastal Lagoon Salt Marsh: Implications for Seasonal Storage and Dispersal. *Estuaries and Coasts*, *34*(3), 470–482. https://doi.org/10.1007/s12237-011-9379-5

Engle, M. A., Tate, M. T., Krabbenhoft, D. P., Schauer, J. J., Kolker, A., Shanley, J. B., & Bothner, M. H. (2010). Comparison of atmospheric mercury speciation and deposition at nine sites across central and eastern North America. *Journal of Geophysical Research Atmospheres*, *115*(18). https://doi.org/10.1029/2010JD014064

Enrico, M., Balcom, P., Johnston, D. T., Foriel, J., & Sunderland, E. M. (2021). Simultaneous combustion preparation for mercury isotope analysis and detection of total mercury using a direct mercury analyzer. *Analytica Chimica Acta*, *1154*. https://doi.org/10.1016/j.aca.2021.338327

Enrico, M., Roux, G. Le, Marusczak, N., Heimbürger, L. E., Claustres, A., Fu, X., … Sonke, J. E. (2016). Atmospheric Mercury Transfer to Peat Bogs Dominated by Gaseous Elemental Mercury Dry Deposition. *Environmental Science and Technology*, *50*(5), 2405–2412. https://doi.org/10.1021/acs.est.5b06058

Estrade, N., Carignan, J., & Donard, O. F. X. (2011). Tracing and quantifying anthropogenic mercury sources in soils of northern France using isotopic signatures. *Environmental Science and Technology*, *45*(4), 1235–1242. https://doi.org/10.1021/es1026823

Evers, D. C., Han, Y.-J., Driscoll, C. T., Kamman, N. C., Goodale, M. W., Lambert, K. F., … Butler, T. (2007). Biological Mercury Hotspots in the Northeastern United States and Southeastern Canada. *BioScience*, *57*(1), 29–43. https://doi.org/10.1641/b570107

Forbrich, I., Giblin, A. E., & Hopkinson, C. S. (2018). Constraining Marsh Carbon Budgets Using Long-Term C Burial and Contemporary Atmospheric CO2 Fluxes. *Journal of Geophysical Research: Biogeosciences*, *123*(3), 867–878. https://doi.org/10.1002/2017JG004336

Garcia-Ordiales, E., Roqueñí, N., & Loredo, J. (2020). Mercury bioaccumulation by Juncus maritimus grown in a Hg contaminated salt marsh (northern Spain). *Marine Chemistry*, *226*, 103859. https://doi.org/10.1016/j.marchem.2020.103859

Graydon, J. A., St. Louis, V. L., Hintelmann, H., Lindberg, S. E., Sandilands, K. A., Rudd, J. W. M., … Lehnherr, I. (2009). Investigation of uptake and retention of atmospheric Hg(II) by boreal forest plants using stable Hg isotopes. *Environmental Science and Technology*, *43*(13), 4960–4966. https://doi.org/10.1021/es900357s

Grigal, D. F. (2003). Mercury Sequestration in Forests and Peatlands. *Journal of Environmental Quality*, *32*(2), 393–405. https://doi.org/10.2134/jeq2003.3930

Grigal, D. F., Kolka, R. K., Fleck, J. A., & Nater, E. A. (2000). Mercury budget of an upland-peatland watershed. *Biogeochemistry*, *50*(1), 95–109. https://doi.org/10.1023/A:1006322705566

Hartman, J., Caswell, H., & Valiela, I. (1983). Effects of wrack accumulation on salt marsh vegetation. *Oceanologica Acta, Actes 17e*(February), 99–102.

He, L., Chen, J. M., Pan, Y., Birdsey, R., & Kattge, J. (2012). Relationships between net primary productivity and forest stand age in U.S. forests. *Global Biogeochemical Cycles*, *26*(3). https://doi.org/10.1029/2010GB003942

Heller, A. A., & Weber, J. H. (1998). Seasonal study of speciation of mercury(II) and monomethylmercury in Spartina alterniflora

from the Great Bay Estuary, NH. *Science of the Total Environment*, *221*(2–3), 181–188. https://doi.org/10.1016/S0048-9697(98)00285-X

Hopkinson, C. S., Morris, J. T., Fagherazzi, S., Wollheim, W. M., & Raymond, P. A. (2018). Lateral Marsh Edge Erosion as a Source of Sediments for Vertical Marsh Accretion. *Journal of Geophysical Research: Biogeosciences*, *123*(8), 2444–2465. https://doi.org/10.1029/2017JG004358

Huang, Q., Chen, J., Huang, W., Fu, P., Guinot, B., Feng, X., … Yu, B. (2016). Isotopic composition for source identification of mercury in atmospheric fine particles. *Atmospheric Chemistry and Physics*, *16*(18), 11773–11786. https://doi.org/10.5194/acp-16-11773-2016

Huang, S., Jiang, R., Song, Q., Zhang, Y., Huang, Q., Su, B., … Lin, H. (2020). Study of mercury transport and transformation in mangrove forests using stable mercury isotopes. *Science of the Total Environment*, *704*, 135928. https://doi.org/10.1016/j.scitotenv.2019.135928

Iverfeldt, Å. (1991). Mercury in forest canopy throughfall water and its relation to atmospheric deposition. *Water Air & Soil Pollution*, *56*(1), 553–564. https://doi.org/10.1007/BF00342299

Jackson, A. K., Evers, D. C., Etterson, M. A., Condon, A. M., Folsom, S. B., Detweiler, J., … Cristol, D. A. (2011). Mercury Exposure Affects The Reproductive Success of a Free-living Terrestrial Songbird, the Carolina Wren (Thryothorus Ludovicianus). In *The Auk* (Vol. 128). https://doi.org/10.1525/auk.2011.11106

Jiskra, M., Heimbürger-Boavida, L.-E., Desgranges, M.-M., Petrova, M. V., Dufour, A., Ferreira-Araujo, B., … Sonke, J. E. (2021). Mercury stable isotopes constrain atmospheric sources to the ocean. *Nature*, *597*(7878), 678–682. https://doi.org/10.1038/s41586-021-03859-8

Jiskra, M., Sonke, J. E., Obrist, D., Bieser, J., Ebinghaus, R., Myhre, C. L., … Dommergue, A. (2018). A vegetation control on seasonal variations in global atmospheric mercury concentrations. *Nature Geoscience*, *11*(4), 244–250. https://doi.org/10.1038/s41561-018-0078-8

Jiskra, M., Wiederhold, J. G., Skyllberg, U., Kronberg, R. M., Hajdas, I., & Kretzschmar, R. (2015). Mercury Deposition and Re-emission Pathways in Boreal Forest Soils Investigated with Hg Isotope Signatures. *Environmental Science and Technology*, *49*(12), 7188–7196. https://doi.org/10.1021/acs.est.5b00742

Jiskra, M., Wiederhold, J. G., Skyllberg, U., Kronberg, R. M., & Kretzschmar, R. (2017). Source tracing of natural organic matter bound mercury in boreal forest runoff with mercury stable isotopes. *Environmental Science: Processes and Impacts*, *19*(10), 1235–1248. https://doi.org/10.1039/c7em00245a

Kirschner, A. S., & Zinnert, J. C. (2020). Two low-lying coastal grassland species differ in mechanistic response to saline flooding stress. *Plant Ecology*, *221*(6), 475–485. https://doi.org/10.1007/s11258-020-01026-z

Kraus, M. L., Weis, P., & Crow, J. H. (1986). The excretion of heavy metals by the salt marsh cord grass,Spartina alterniflora, and Spartina's role in mercury cycling. *Marine Environmental Research*, *20*(4), 307–316. https://doi.org/10.1016/0141-1136(86)90056-5

Kwon, S. Y., Blum, J. D., Chen, C. Y., Meattey, D. E., & Mason, R. P. (2014). Mercury isotope study of sources and exposure pathways of methylmercury in estuarine food webs in the northeastern U.S. *Environmental Science and Technology*, *48*(17), 10089–10097. https://doi.org/10.1021/es5020554

Kwon, S. Y., Blum, J. D., Yin, R., Tsui, M. T. K., Yang, Y. H., & Choi, J. W. (2020). Mercury stable isotopes for monitoring the effectiveness of the Minamata Convention on Mercury. *Earth-Science Reviews*, *203*(January), 103111. https://doi.org/10.1016/j.earscirev.2020.103111

Lane, O., Adams, E. M., Pau, N., O'Brien, K. M., Regan, K., Farina, M., … Zarudsky, J. (2020). Long-term monitoring of mercury

in adult saltmarsh sparrows breeding in Maine, Massachusetts and New York, USA 2000–2017. In *Ecotoxicology* (Vol. 29). https://doi.org/10.1007/s10646-020-02180-w

Lane, O. P., O'Brien, K. M., Evers, D. C., Hodgman, T. P., Major, A., Pau, N., … Perry, D. (2011). Mercury in breeding saltmarsh sparrows (Ammodramus caudacutus caudacutus). *Ecotoxicology*, *20*(8), 1984–1991. https://doi.org/10.1007/s10646-011-0740-z

Lepak, R. F., Yin, R., Krabbenhoft, D. P., Ogorek, J. M., DeWild, J. F., Holsen, T. M., & Hurley, J. P. (2015). Use of Stable Isotope Signatures to Determine Mercury Sources in the Great Lakes. *Environmental Science & Technology Letters*, *2*(12), 335–341. https://doi.org/10.1021/acs.estlett.5b00277

Liu, M., Zhang, Q., Maavara, T., Liu, S., Wang, X., & Raymond, P. A. (2021). Rivers as the largest source of mercury to coastal oceans worldwide. *Nature Geoscience*, *14*(9), 672–677. https://doi.org/10.1038/s41561-021-00793-2

Louis, V. L. S. T., Rudd, J. W. M., Kelly, C. A., Hall, B. D., Rolfhus, K. R., Scott, K. J., … Dong, W. (2001). Importance of the forest canopy to fluxes of methyl mercury and total mercury to boreal ecosystems. *Environmental Science and Technology*, *35*(15), 3089–3098. https://doi.org/10.1021/es001924p

Mann, K. H. (1988). Production and use of detritus in various freshwater, estuarine, and coastal marine ecosystems. *Limnology and Oceanography*, *33*(4part2), 910–930. https://doi.org/10.4319/LO.1988.33.4PART2.0910

Mao, Y., Li, Y., Richards, J., & Cai, Y. (2013). Investigating uptake and translocation of mercury species by sawgrass (Cladium jamaicense) using a stable isotope tracer technique. *Environmental Science and Technology*, *47*(17), 9678–9684. https://doi.org/10.1021/es400546s

Maricle, B. R., Koteyeva, N. K., Voznesenskaya, E. V., Thomasson, J. R., & Edwards, G. E. (2009). Diversity in leaf anatomy, and stomatal distribution and conductance, between salt marsh and freshwater species in the C4 genus Spartina (Poaceae). *New Phytologist*, *184*(1), 216–233. https://doi.org/10.1111/J.1469-8137.2009.02903.X

Marques, B., Lillebø, A. I., Pereira, E., & Duarte, A. C. (2011). Mercury cycling and sequestration in salt marshes sediments: An ecosystem service provided by Juncus maritimus and Scirpus maritimus. *Environmental Pollution*, *159*(7), 1869–1876. https://doi.org/10.1016/j.envpol.2011.03.036

Meng, M., Sun, R. Y., Liu, H. W., Yu, B., Yin, Y. G., Hu, L. G., … Jiang, G. Bin. (2019). An Integrated Model for Input and Migration of Mercury in Chinese Coastal Sediments. *Environmental Science and Technology*, *53*(5), 2460–2471. https://doi.org/10.1021/acs.est.8b06329

Millette, T. L., Argow, B. A., Marcano, E., Hayward, C., Hopkinson, C. S., & Valentine, V. (2010). Salt Marsh Geomorphological Analyses via Integration of Multitemporal Multispectral Remote Sensing with LIDAR and GIS . *Journal of Coastal Research*, *265*, 809–816. https://doi.org/10.2112/jcoastres-d-09-00101.1

Millhollen, A. G., Gustin, M. S., & Obrist, D. (2006). Foliar Mercury Accumulation and Exchange for Three Tree Species. *Environmental Science & Technology*, *40*(19), 6001–6006. https://doi.org/10.1021/es0609194

Morris, J. T. (2007). Estimating Net Primary Production of Salt Marsh Macrophytes. In *Principles and Standards for Measuring Primary Production* (Vol. 15, pp. 106–119). https://doi.org/10.1093/acprof:oso/9780195168662.003.0007

Morris, J. T., Sundberg, K., & Hopkinson, C. S. (2013). Salt marsh primary production and its responses to relative sea level and nutrientsin estuaries at plum island, Massachusetts, and North Inlet, South Carolina, USA. *Oceanography*, *26*(3), 78–84. https://doi.org/10.5670/oceanog.2013.48

Muench, A., & Elsey-Quirk, T. (2019). Competitive reversal between plant species is driven by species-specific tolerance to flooding stress and nutrient acquisition during early marsh succession. *J Appl Ecol*, *56*, 2236–2247. https://doi.org/10.1111/1365-2664.13458

NADP. (2017). National Atmospheric Deposition Program, Mercury Deposition Network. Retrieved from http://nadp.slh.wisc.edu/maplib/pdf/mdn/hg_Conc_2017.pdf

NOAA. (2020). National Oceanic and Atmospheric Administration Tide Predictions. Retrieved from https://www.tidesandcurrents.noaa.gov/noaatidepredictions.html?id=8441241

Obrist, D., Agnan, Y., Jiskra, M., Olson, C. L., Colegrove, D. P., Hueber, J., … Helmig, D. (2017). Tundra uptake of atmospheric elemental mercury drives Arctic mercury pollution. *Nature*, *547*(7662), 201–204. https://doi.org/10.1038/nature22997

Obrist, D., Kirk, J. L., Zhang, L., Sunderland, E. M., Jiskra, M., & Selin, N. E. (2018). A review of global environmental mercury processes in response to human and natural perturbations: Changes of emissions, climate, and land use. *Ambio*, *47*(2), 116–140. https://doi.org/10.1007/s13280-017-1004-9

Obrist, D., Roy, E. M., Harrison, J. L., Kwong, C. F., William Munger, J., Moosmüller, H., … Commane, R. (2021). Previously unaccounted atmospheric mercury deposition in a midlatitude deciduous forest. *Proceedings of the National Academy of Sciences of the United States of America*, *118*(29). https://doi.org/10.1073/pnas.2105477118

Ouyang, X., Lee, S. Y., & Connolly, R. M. (2017). The role of root decomposition in global mangrove and saltmarsh carbon budgets. *Earth-Science Reviews*, Vol. 166, pp. 53–63. https://doi.org/10.1016/j.earscirev.2017.01.004

Raymond, P. A., & Hopkinson, C. S. (2003). Ecosystem Modulation of Dissolved Carbon Age in a Temperate Marsh-Dominated Estuary. *Ecosystems*, *6*(7), 694–705. https://doi.org/10.1007/s10021-002-0213-6

Risch, M. R., DeWild, J. F., Gay, D. A., Zhang, L., Boyer, E. W., & Krabbenhoft, D. P. (2017). Atmospheric mercury deposition to forests in the eastern USA. *Environmental Pollution*, *228*, 8–18. https://doi.org/10.1016/j.envpol.2017.05.004

Sun, L., Shao, D., Xie, T., Gao, W., Ma, X., Ning, Z., & Cui, B. (2020). How does Spartina alterniflora invade in salt marsh in relation to tidal channel networks? Patterns and processes. *Remote Sensing*, *12*(18). https://doi.org/10.3390/RS12182983

Tobias, C., & Neubauer, S. (2009). Salt Marsh Biogeochemistry - An Overview. In G. M. E. Perillo, E. Wolanski, D. R. Cahoon, & M. M. Brinson (Eds.), *Coastal Wetlands: An Integrated Ecosystem Approach* (pp. 1–57). Amsterdam, the Netherlands: Elsevier.

Tobias, Craig, & Neubauer, S. C. (2019). Salt Marsh Biogeochemistry—An Overview. *Coastal Wetlands: An Integrated Ecosystem Approach*, 539–596. https://doi.org/10.1016/B978-0-444-63893-9.00016-2

U.S. EPA. (1998). Method 7473, Mercury in solids and solutions by thermal decomposition, amalgamation, and atomic absorption spectrophotometry. In *Revision 0. Washington, DC.*

Valiela, I., Teal, J. M., & Persson, N. Y. (1976). Production and dynamics of experimentally enriched salt marsh vegetation: Belowground biomass. *Limnology and Oceanography*, *21*(2), 245–252. https://doi.org/10.4319/lo.1976.21.2.0245

Visser, J. M., Midway, S., Baltz, D. M., & Sasser, C. E. (2018). Ecosystem structure of tidal saline marshes. In *Coastal Wetlands: An Integrated Ecosystem Approach* (pp. 519–538). https://doi.org/10.1016/B978-0-444-63893-9.00015-0

Wang, J. J., Guo, Y. Y., Guo, D. L., Yin, S. L., Kong, D. L., Liu, Y. S., & Zeng, H. (2012). Fine root mercury heterogeneity: Metabolism of lower-order roots as an effective route for mercury removal. *Environmental Science and Technology*, *46*(2), 769–777. https://doi.org/10.1021/es2018708

Wang, T., & Obrist, D. (2022). Inorganic and methylated mercury dynamics in estuarine water of a salt marsh in Massachusetts, USA. *Environmental Pollution*, *294*. https://doi.org/10.1016/j.envpol.2021.118657

Wang, X., Bao, Z., Lin, C. J., Yuan, W., & Feng, X. (2016). Assessment of Global Mercury Deposition through Litterfall. *Environmental Science and Technology*, *50*(16), 8548–8557. https://doi.org/10.1021/acs.est.5b06351

Wang, X., Yuan, W., Lin, C. J., Luo, J., Wang, F., Feng, X., … Liu, C. (2020). Underestimated Sink of Atmospheric Mercury in a Deglaciated Forest Chronosequence. *Environmental Science and Technology*, *54*(13), 8083–8093. https://doi.org/10.1021/acs.est.0c01667

Wang, Y., Wang, Z., Zheng, X., & Zhou, L. (2021). Influence of Spartina alterniflora invasion on mercury storage and methylation in the sediments of Yangtze River estuarine wetlands. *Estuarine, Coastal and Shelf Science*, *265*(June 2021), 107717. https://doi.org/10.1016/j.ecss.2021.107717

Washburn, S. J., Blum, J. D., Demers, J. D., Kurz, A. Y., & Landis, R. C. (2017). Isotopic Characterization of Mercury Downstream of Historic Industrial Contamination in the South River, Virginia. *Environmental Science and Technology*, *51*(19), 10965–10973. https://doi.org/10.1021/acs.est.7b02577

Weis, J. S., & Weis, P. (2004). Metal uptake, transport and release by wetland plants: implications for phytoremediation and restoration. *Environment International*, *30*(5), 685–700. https://doi.org/10.1016/j.envint.2003.11.002

Wilson, C. A., Hughes, Z. J., FitzGerald, D. M., Hopkinson, C. S., Valentine, V., & Kolker, A. S. (2014). Saltmarsh pool and tidal creek morphodynamics: Dynamic equilibrium of northern latitude saltmarshes? *Geomorphology*, *213*, 99–115. https://doi.org/10.1016/j.geomorph.2014.01.002

Windham, L, Weis, J. ., & Weis, P. (2003). Uptake and distribution of metals in two dominant salt marsh macrophytes, Spartina alterniflora (cordgrass) and Phragmites australis (common reed). *Estuarine, Coastal and Shelf Science*, *56*(1), 63–72. https://doi.org/10.1016/S0272-7714(02)00121-X

Windham, Lisamarie. (2001). Comparison of biomass production and decomposition between Phragmites australis (common reed) and spartina patens (salt hay grass) in brackish tidal marshes of New Jersey, USA. *Wetlands*, *21*(2), 179–188. https://doi.org/10.1672/0277-5212(2001)021[0179:COBPAD]2.0.CO;2

Windham, Lisamarie, Wei, J. S., & Weis, P. (2001). *Patterns and Processes of Mercury Release from Leaves of Two Dominant Salt Marsh Macrophytes , Phragmites australis and Spartina alterniflora*. *24*(6), 787–795. https://doi.org/https://doi.org/10.2307/1353170

Windham, Lisamarie, Weis, J. S., & Weis, P. (2001). Patterns and processes of mercury release from leaves of two dominant salt marsh macrophytes, Phragmites australis and Spartina alterniflora. *Estuaries*, *24*(6 A), 787–795. https://doi.org/10.2307/1353170

Windham, Lisamarie, Weis, J. S., Weis, P., Wei, J. S., Weis, P., Weis, J. S., & Weis, P. (2001). Patterns and Processes of Mercury Release from Leaves of Two Dominant Salt Marsh Macrophytes , Phragmites australis and Spartina alterniflora. *Estuaries*, *24*(6), 787–795. https://doi.org/https://doi.org/10.2307/1353170

Woerndle, G. E., Tsz-Ki Tsui, M., Sebestyen, S. D., Blum, J. D., Nie, X., & Kolka, R. K. (2018). New Insights on Ecosystem Mercury Cycling Revealed by Stable Isotopes of Mercury in Water Flowing from a Headwater Peatland Catchment. *Environmental Science and Technology*, *52*(4), 1854–1861. https://doi.org/10.1021/acs.est.7b04449

Wohlgemuth, L., Rautio, P., Ahrends, B., Russ, A., Vesterdal, L., Waldner, P., … Jiskra, M. (2022). Physiological and climate controls on foliar mercury uptake by European tree species. *Biogeosciences*, *19*, 1335–1353. https://doi.org/10.5194/bg-19-1335-2022

Wolanski, E., Perillo, G. M. E., Brinson, M. M., & Cahoon, D. R. (2009). *Coastal Wetlands: A Synthesis*. Retrieved from http://www.elsevier.com

Yin, R., Feng, X., & Meng, B. (2013). Stable mercury isotope variation in rice plants (Oryza sativa L.) from the Wanshan mercury Mining District, SW China. *Environmental Science and Technology*, *47*(5), 2238–2245. https://doi.org/10.1021/es304302a

Yu, B., Fu, X., Yin, R., Zhang, H., Wang, X., Lin, C. J., … Feng, X. (2016). Isotopic composition of atmospheric mercury in China: New evidence for sources and transformation processes in air and in vegetation. *Environmental Science and Technology*, *50*(17), 9362–9369. https://doi.org/10.1021/acs.est.6b01782

Yuan, W., Wang, X., Lin, C. J., Sommar, J., Lu, Z., & Feng, X. (2019). Process factors driving dynamic exchange of elemental mercury vapor over soil in broadleaf forest ecosystems. *Atmospheric Environment*, *219*.

https://doi.org/10.1016/j.atmosenv.2019.117047

Zawislanski, P. T., Mountford, H., Wong, H. C., Sears, T. C., & Chau, S. (2001). Accumulation of selenium and trace metals on plant litter in a tidal marsh. *Estuarine, Coastal and Shelf Science*, *52*(5), 589–603. https://doi.org/10.1006/ecss.2001.0772

Zheng, W., Obrist, D., Weis, D., & Bergquist, B. A. (2016). Mercury isotope compositions across North American forests. *Global Biogeochemical Cycles*, *30*(10), 1475–1492. https://doi.org/10.1002/2015GB005323

Zhou, J., & Obrist, D. (2021). Global Mercury Assimilation by Vegetation. *Environmental Science and Technology*, *55*(20), 14245–14257. https://doi.org/10.1021/acs.est.1c03530

Zhou, J., Obrist, D., Dastoor, A., Jiskra, M., & Ryjkov, A. (2021). Vegetation uptake of mercury and impacts on global cycling. *Nature Reviews Earth & Environment*, *2*(4), 269–284. https://doi.org/10.1038/s43017-021-00146-y

https://doi.org/10.5194/egusphere-2023-720
Preprint. Discussion started: 8 May 2023

Figures and tables

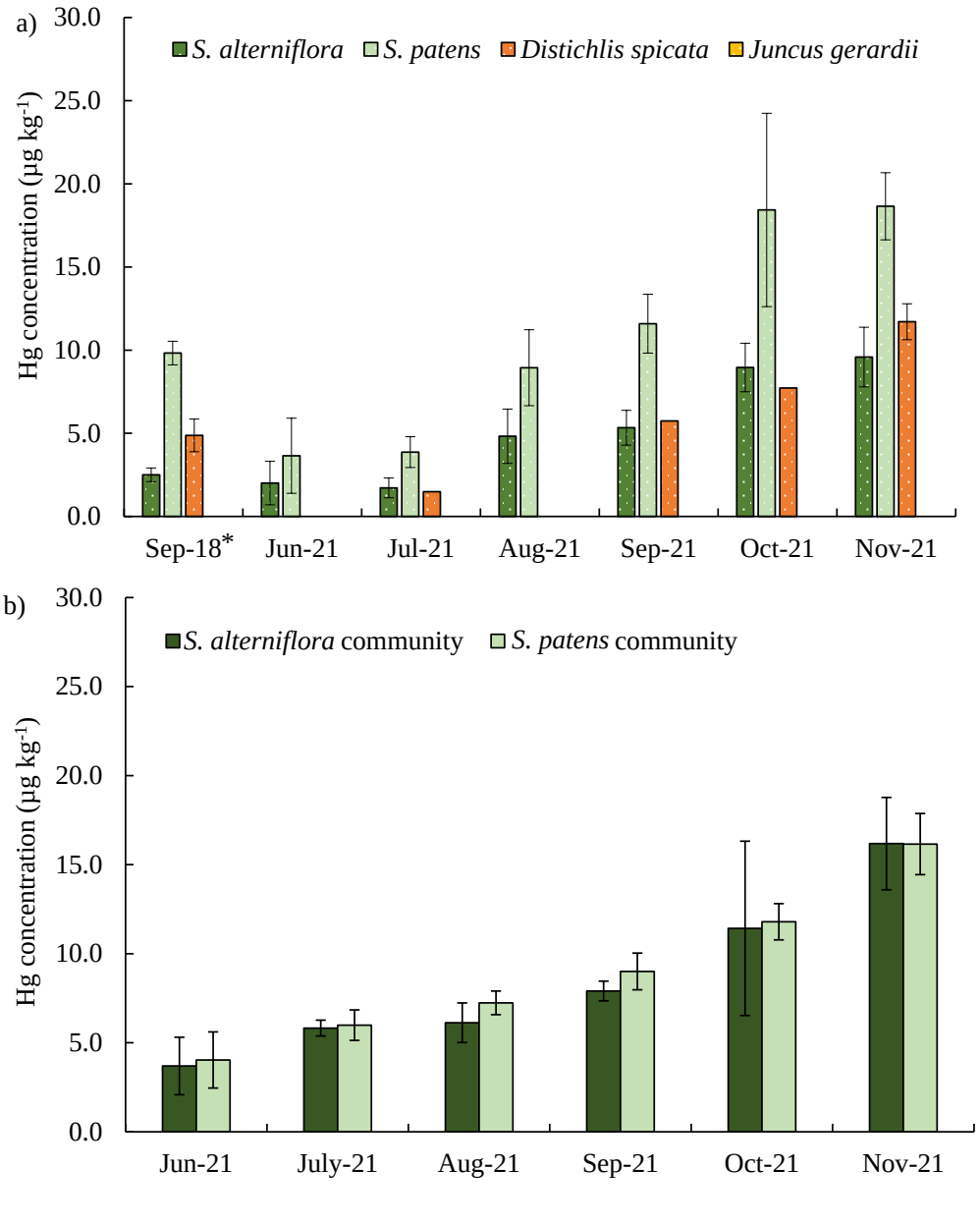

Figure 1. Seasonal Hg concentrations of the four dominated salt marsh live plant species in 2018 and 2021 a), and seasonal Hg concentrations of the *S. alterniflora* and *S. patens* communities in 2021 b). Different colors indicate different plant species. Standard errors indicate four replicates. *: Standard errors indicate duplicates for a sample.

https://doi.org/10.5194/egusphere-2023-720
Preprint. Discussion started: 8 May 2023

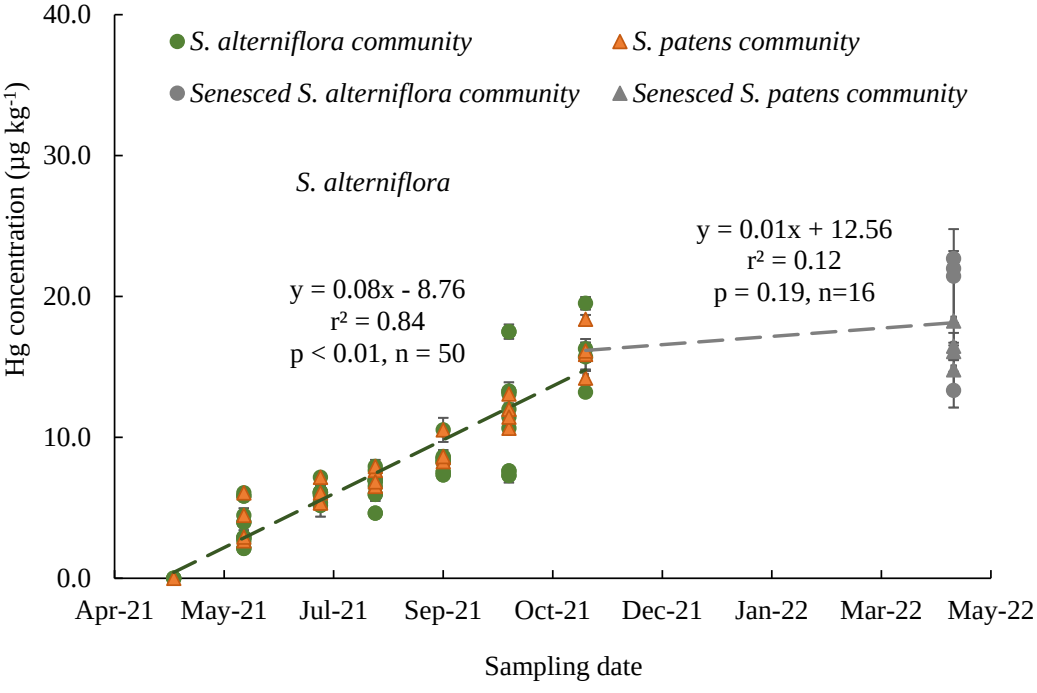

723

724 **Figure 2. Hg concentrations of live and senesced aboveground biomass of S. alterniflora and S. patens communities corresponds with**
725 **sampling dates in 2021. Green circles indicate live S. alterniflora communities, orange triangles indicate live S. patens communities, grey**
726 **circles indicate senesced S. alterniflora communities, and grey triangles indicate senesced S. patens communities. Standard errors**
727 **indicate four replicates.**

728

729

https://doi.org/10.5194/egusphere-2023-720
Preprint. Discussion started: 8 May 2023

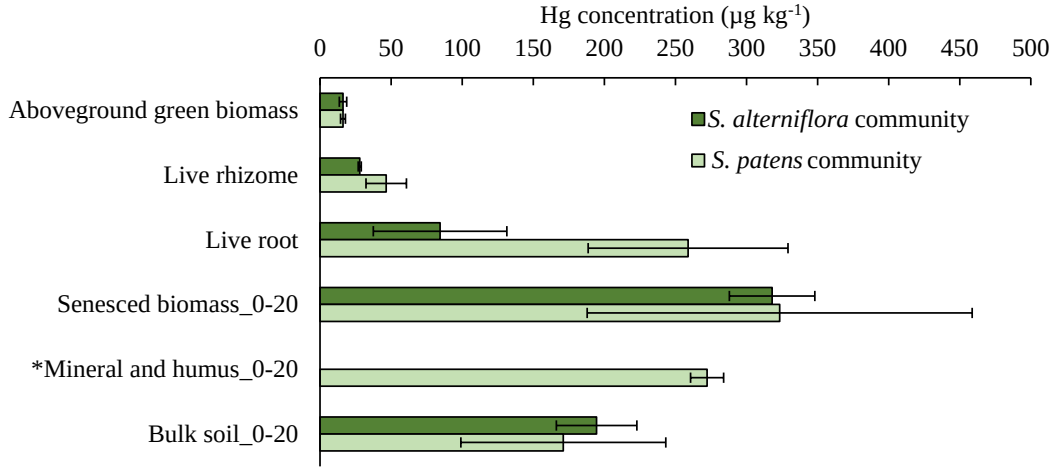

730

731 **Figure 3. Hg concentrations in live above- and belowground biomass of *S. alterniflora* and *S. patens* communities, as well as Hg**
732 **concentrations of minerals and humus and bulk soils up to depth of 20cm covered by these two plant species. Dark green columns denote**
733 ***S. alterniflora* community, light green columns denote *S. patens* community. Standard errors indicate multiple sample analysis. *Hg**
734 **concentration in mineral and humus only present one site covered by *S. patens*, and standard errors are duplicates.**

https://doi.org/10.5194/egusphere-2023-720
Preprint. Discussion started: 8 May 2023

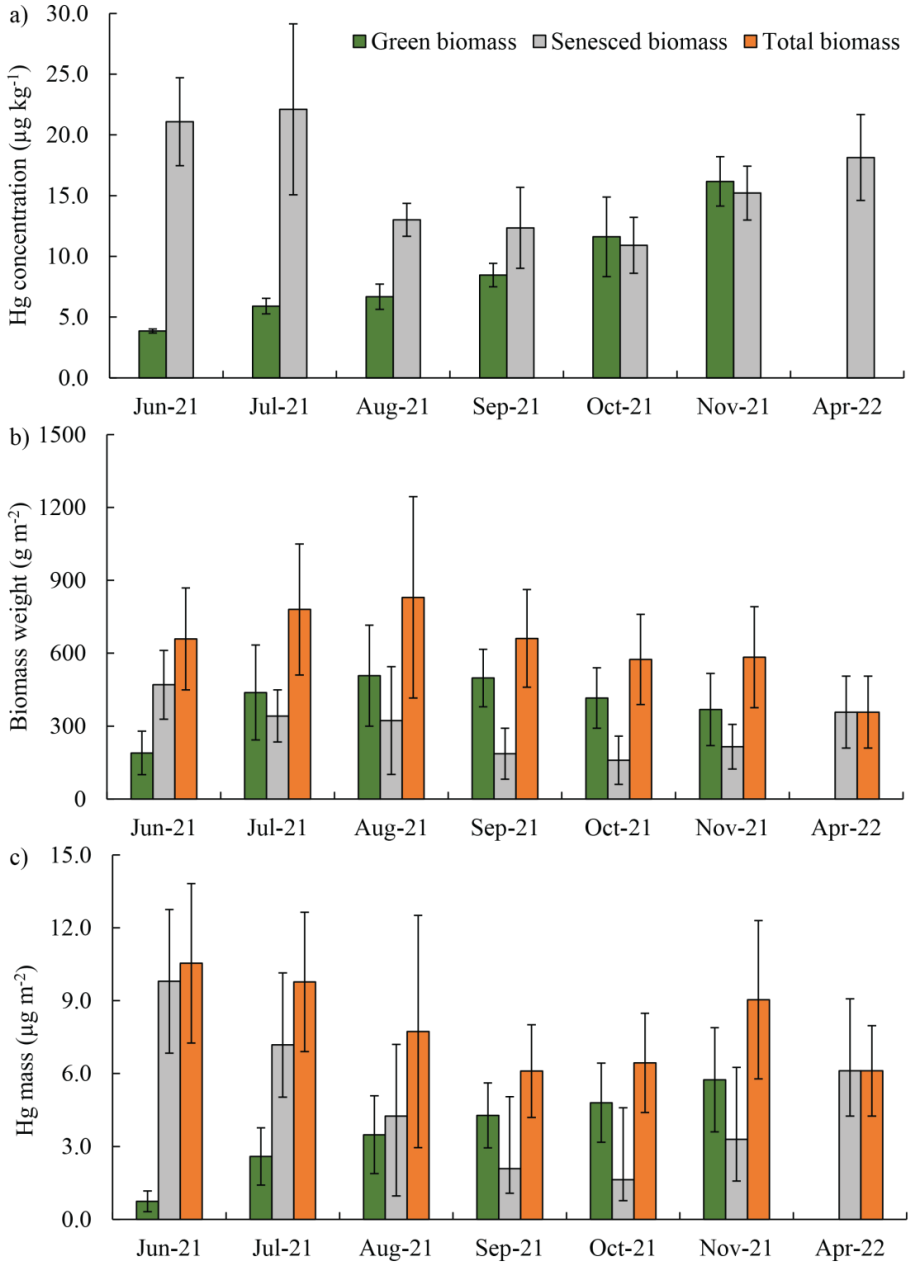

Figure 4 Seasonal patterns of Hg concentrations a), biomass dry weight b), and Hg mass c) in aboveground live and senesced biomass from June 2021 to April 2022. The green columns represent live biomass, grey columns represent senesced biomass, and orange columns represent total biomass weight and Hg mass of adding live and senesced biomass. Standard errors indicate four replicates.

https://doi.org/10.5194/egusphere-2023-720
Preprint. Discussion started: 8 May 2023

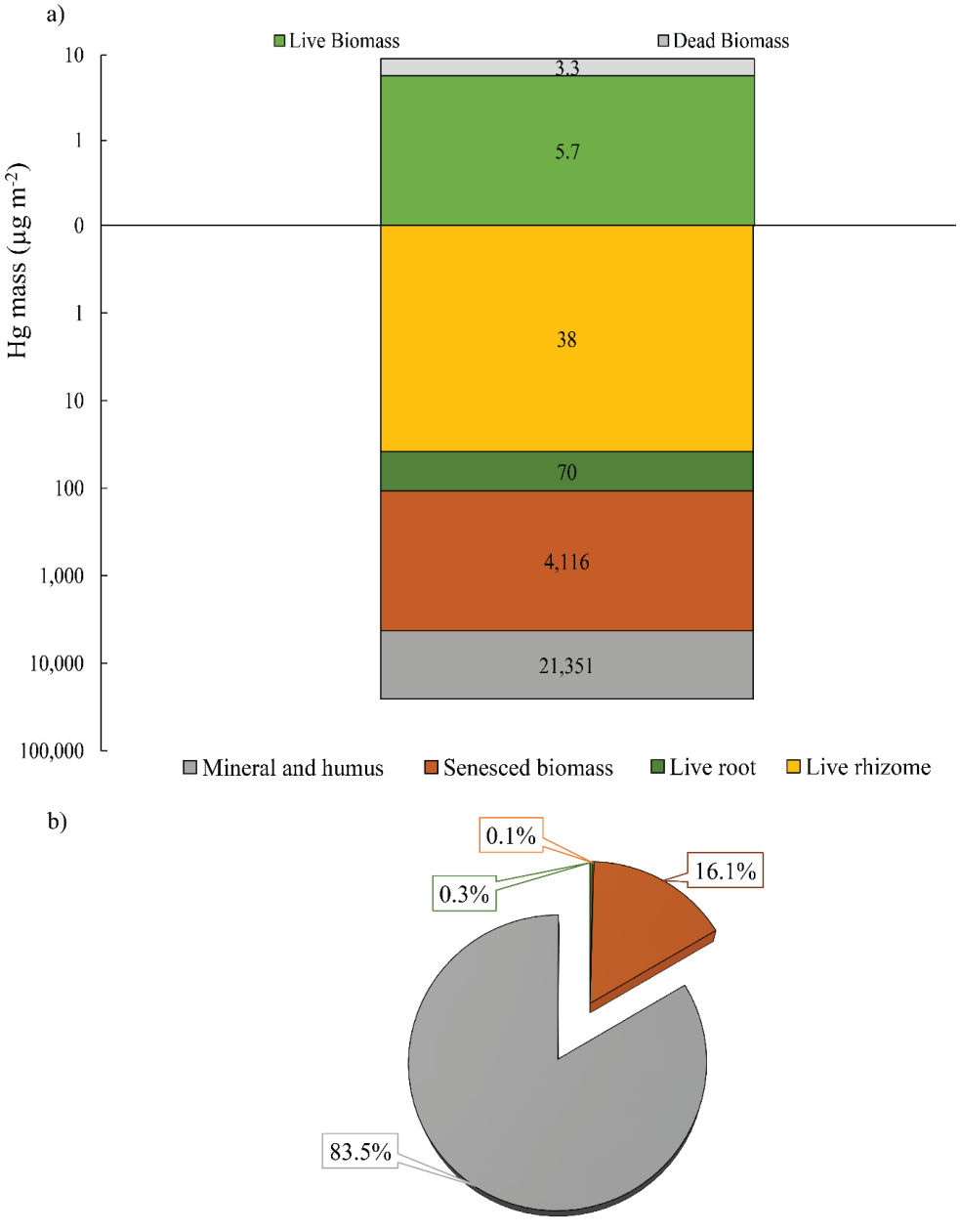

739

740 **Figure 5. Hg mass of above- and belowground biomass, including live and senesced biomass, and mineral and humus fractions in a soil**
741 **depth of 40cm, a), and percentages of Hg mass contribution from belowground sections to the Hg soil pool of a soil depth of 40cm, b).**
742 **Different colors indicate of different sections of the marsh.**

743

https://doi.org/10.5194/egusphere-2023-720
Preprint. Discussion started: 8 May 2023

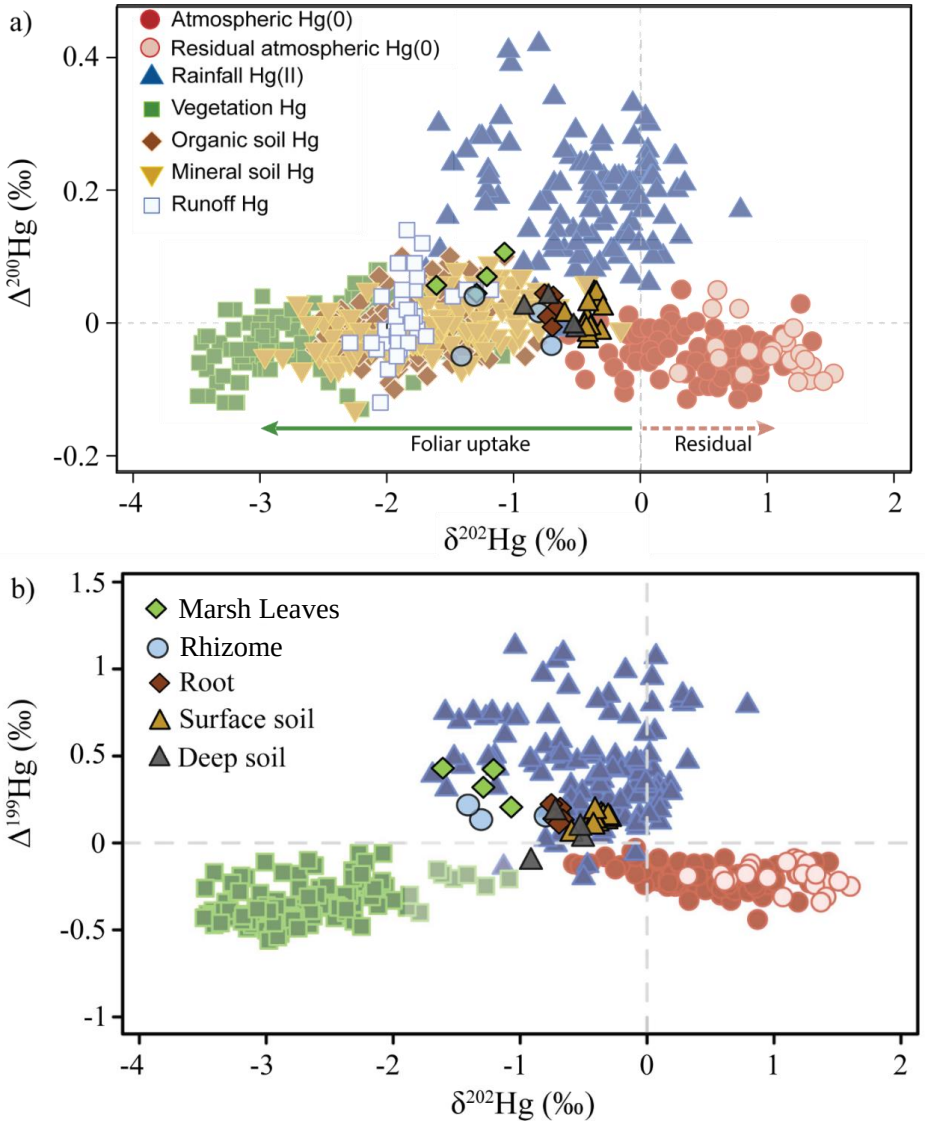

744

745 **Figure 6. Hg isotopes in salt marsh plants and soils, and foliage a) of Δ^{200}Hg and δ^{202}Hg, and b) of Δ^{199}Hg and δ^{202}Hg. Composition of**
746 **Hg sources in marsh vegetation and soils (surface and deep soil layers), and all previously published currently available isotope data of**
747 **sources of Hg in vegetation and in terrestrial sinks, atmospheric Hg(0) and Hg(II) sources (Zhou et al., 2021), plotted as a) even-mass-**
748 **independent (Δ^{200}Hg) versus mass- dependent (δ^{202}Hg) isotopes a) and b) odd-mass-independent (Δ^{199}Hg) versus mass- dependent**
749 **(δ^{202}Hg) isotopes.**

750

https://doi.org/10.5194/egusphere-2023-720
Preprint. Discussion started: 8 May 2023

751

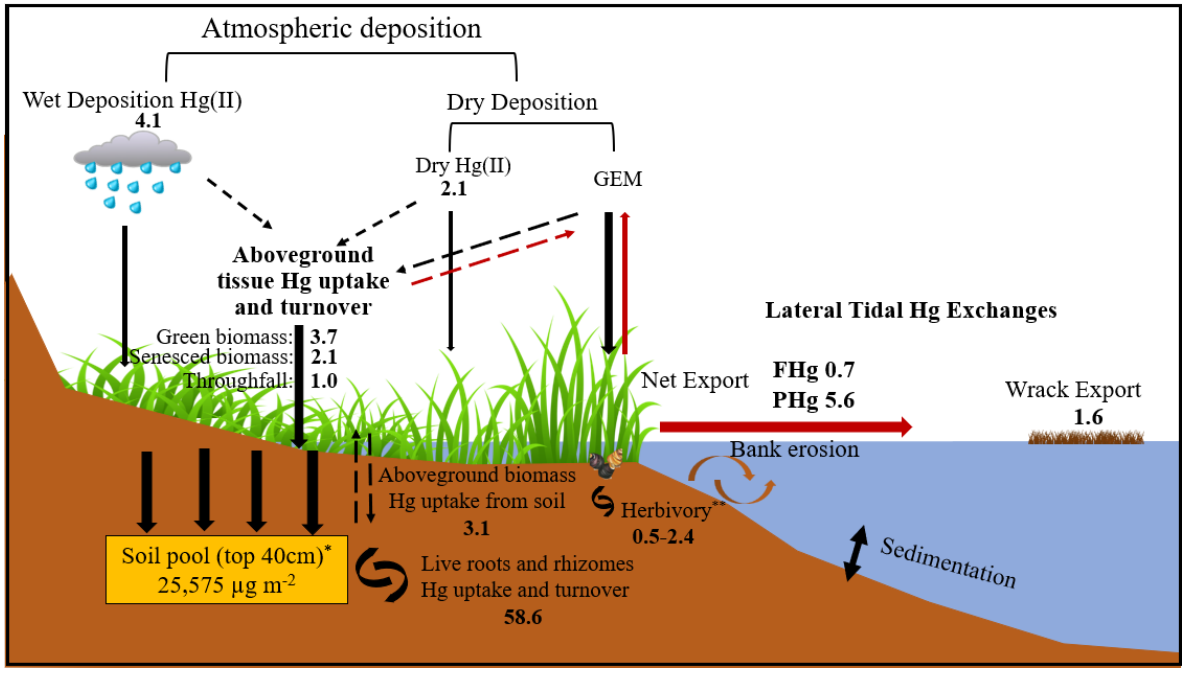

752

753 **Figure 7. Hg mass balance of the study salt marsh ecosystem. The values shown mostly represent the median Hg flux values with unit**
754 **of µg m^{-2} yr^{-1}, except for the soil pool*, which represents an averaged value, and herbivory**, which indicates a range. The red arrows**
755 **indicate the emission of Hg back to the atmosphere and its export out of the salt marsh.**

756

https://doi.org/10.5194/egusphere-2023-720
Preprint. Discussion started: 8 May 2023

Table 1 Hg mass balance of the study salt marsh ecosystem.

	Category		Item	Hg flux ($\mu g\ m^{-2}\ yr^{-1}$)	Percent of Hg sources	Reference	Hg fluxes scaled to the marsh ($kg\ yr^{-1}$)*
Present-day Hg Mass Balance (total inputs minus exports)	Deposition		Green aboveground biomass*	3.7±1.4 (1.3-5.0)	65% atmospheric Hg	This study	0.15 (0.05-0.20)
			Senesced aboveground biomass*	2.1±1.1 (1.2-4.7)	65% atmospheric Hg	This study	0.08 (0.05-0.19)
			Total aboveground biomass	5.9±2.1 (3.1-9.7)	65% atmospheric Hg	This study	0.24(0.12-0.39)
			Throughfall	1.0±0.4 (0.5-1.6)	100% atmospheric Hg	This study	0.04(0.02-0.06)
			Wet Hg(II)	4.1 (2.9-5.2)	100% atmospheric Hg	(Engle et al. 2010, NADP, 2017)	0.16 (0.12- 0.21)
			Dry Hg(II)	2.1 (1.2-3.0)	100% atmospheric Hg	(Engle et al., 2010, Obrist et al., 2021)	0.08 (0.05-0.12)
	Total			13.1 (7.7-19.5)		This study	0.52 (0.31-0.78)
	Export		Tidal export dissolved Hg	0.7	100% marsh soil Hg	Wang and Obrist, 2022	0.03
			Tidal export particulate Hg	5.6	100% marsh soil Hg	Wang and Obrist, 2023	0.22
			Wrack	1.6 (1.4-1.7)	100% marsh plants	This study	0.06 (0.06-0.07)
	Total			7.9 (7.7 - 8.0)		This study	0.32 (0.31-0.32)
	Net mass accumulation (estimated total deposition – total export)			**5.2 (0-11.5)**		**This study**	**0.21 (0.0-0.46)**
	Internal Cycling		Green aboveground biomass*	1.9±0.7 (0.7-2.6)	35% soil Hg	This study	0.08 (0.03-0.10)
			Senesced aboveground biomass*	1.1±0.6 (0.6-2.5)	35% soil Hg	This study	0.04 (0.02-0.10)
			Total aboveground biomass	3.1±1.1 (1.6-5.1)	35% soil Hg	This study	0.12 (0.06-0.20)
			Roots and rhizomes	58.6 (19.5-253.8)	90% soil Hg	This study	2.3 (0.8-10.2)
			Herbivory	0.5-2.4	100% marsh plants	This study	
			Item	Hg mass ($\mu g\ m^{-2}$)	Percent of Hg sources	Reference	Hg mass scaled to the marsh (kg)*
Total Soil Hg Mass	**Soil Hg mass top 40 cm**			25,575±14,409 (16,127-46,997)		This study	1,023±576 (645-1880)

* Salt marsh area (vegetated): 40 km^2